Chapter 1 Introduction

1.1 Introduction

Autoimmune disorders are diseases that occur when the body produces an inappropriate immune response against its own tissues. Sometimes the immune system will cease to recognize one or more of the body's normal constituents as "self" and will produce autoantibodies – antibodies that attack its own cells, tissues, and/or organs. This causes inflammation and damage and leads to autoimmune disorders. The cause of autoimmune diseases is unknown, but it appears that there is an inherited predisposition in many cases. In a few types of autoimmune disease (such as rheumatic fever), a virus or infection with bacteria triggers an immune response and the antibodies or T-cells attack normal cells because some part of their structure resembles a part of the infecting microorganism (http://labtestsonline.org/understanding/conditions/autoimmune).

Autoimmune disorders fall into two general types: those that damage many organs (systemic autoimmune diseases) and those where only a single organ or tissue is directly damaged by the autoimmune process (localized). However, the distinctions become blurred as the effect of localized autoimmune disorders frequently extends beyond the targeted tissues, indirectly affecting other body organs and systems. In some cases, the antibodies may not be directed at a specific tissue or organ; for example, antiphospholipid antibodies can react with substances (phospholipids) that are the normal constituents of platelets and the outermost layer of cells (cell membranes), which can lead to the formation of blood clots within the blood vessels (thrombosis) (http://labtestsonline.org/understanding/conditions/autoimmune).

1.2 Example of AutoImmune diseases

1.2.1 Glomerulonephritis (Glomerular Disease) is caused by deposition of antigen-antibody complexes in the subendothelial or subepithelial surface of the glomerular basement membrane. Secondary glomerulonephritis occurs as a side effect of chronic infectious, neoplastic, or immunologic disorders. Animals with idiopathic glomerulonephritis (>50% of cases) usually

have signs of renal disease, whereas secondary glomerulonephritis is often a relatively minor part of a more serious disease.

1.2.2 Systemic Lupus Erythematosus (SLE) occurs in dogs, is rare in cats, and has been reported in large animals like humans. It has 2 immunologic features: immune complex disease and heightened antibody responsiveness with a tendency to produce autoantibodies. Therefore, it is a combination of Type II and III diseases. Antibodies to nucleic acid are the diagnostic hallmark of SLE, but in some individuals, antibodies to RBC, platelets, lymphocytes, clotting factors, immunoglobulin (rheumatoid factors), and thyroglobulin also may be present. These autoantibodies, in particular those to nucleic acids, are not always pathogenic by themselves. Rather, they should be considered markers of the disease. Although combinations of autoantibodies and self-antigens may contribute to the total pool of immune complexes, they are not the sole source of immune complexes. Usually, either the immune complex or the autoantibody aspect of the disease predominates in a given animal. Immune complex deposition around small blood vessels leads to synovitis, dermal reactions, oral erosions and ulcers, myositis, neuritis, meningitis, arteritis, myelopathy, glomerulonephritis, and pleuritis.

1.2.3 Hypersensitivity pneumonitis is caused by deposition of immune complexes in the alveoli; it is most common in large animals that are exposed to antigenic dusts. The most potent antigens of this type are those contained in the spores of thermophilic actinomycetes from moldy hay. Inhalation of these spores causes farmer's lung disease in humans and a similar condition in cattle (Hypersensitivity Pneumonitis). Hypersensitivity pneumonitis is characterized by the onset of respiratory distress 4-6 hr after exposure to moldy hay. The most effective treatment is removal of the source of the antigen; otherwise, corticosteroid therapy may help. (http://www.merckvetmanual.com/mvm/index.jsp?cfile=htm/bc/60208.htm).

1.2.4 Rheumatoid Arthritis

Rheumatoid arthritis (RA) is a long-term disease that leads to inflammation of the joints and surrounding tissues. It can also affect other organs. The cause of RA is unknown. It is an autoimmune disease, which means the body's immune system mistakenly attacks healthy tissue. RA can occur at any age, but is more common in middle age. Women get RA more often than

men. Infection, genes, and hormone changes may be linked to the disease. RA usually affects joints on both sides of the body equally. Wrists, fingers, knees, feet, and ankles are the most commonly affected. The disease often begins slowly, usually with only minor joint pain, stiffness, and fatigue. Joint symptoms may include: Morning stiffness, which lasts more than 1 hour, is common. Joints may feel warm, tender, and stiff when not used for an hour. Joint pain is often felt on the same joint on both sides of the body. Over time, joints may lose their range of motion and may become deformed. (http://www.nlm.nih.gov/medlineplus/ency/article/000431).

1.2.5 Type 1 Diabetes

Type 1 diabetes is a lifelong (chronic) disease in which there are high levels of sugar (glucose) in the blood. Type 1 diabetes can occur at any age. However, it is most often diagnosed in children, adolescents, or young adults. Insulin is a hormone produced by special cells, called beta cells, in the pancreas. The pancreas is found behind your stomach. Insulin is needed to move blood sugar (glucose) into cells, where it is stored and later used for energy. In type 1 diabetes, beta cells produce little or no insulin. Without enough insulin, glucose builds up in the bloodstream instead of going into the cells. The body is unable to use this glucose for energy. This leads to the symptoms of type 1 diabetes. The exact cause of type 1 diabetes is unknown. Most likely it is an autoimmune disorder. An infection or some other trigger causes the body to mistakenly attack the cells in the pancreas that make insulin. This kind of disorder can be passed down through families. These symptoms may be the first signs of type 1 diabetes, or may occur when the blood sugar is high, being very thirsty, feeling hungry, feeling tired or fatigued, having blurry eyesight, losing the feeling or feeling tingling in your feet, losing weight without trying, urinating more often. For other people, these warning symptoms may be the first signs of type 1 diabetes, or they may happen when the blood sugar is very high, rapid breathing, dry skin and mouth, flushed face, fruity breath odor, nausea or vomiting, inability to keep down fluids, stomach pain. Low blood sugar (hypoglycemia) can develop quickly in people with diabetes who are taking insulin. Symptoms usually appear when the blood sugar level falls below 70 mg/dL. (www.nlm.nih.gov/medlineplus/ency/article/000305).

1.3 Anatomy of Brachial Artery

The brachial artery is the major blood vessel of the (upper) arm. It is the continuation of the axillary artery beyond the lower margin of teres major muscle. It continues down the ventral surface of the arm until it reaches the cubital fossa at the elbow. It then divides into the radial and ulnar arteries which run down the forearm. In some individuals, the bifurcation occurs much earlier and the ulnar and radial arteries extend through the upper arm. The pulse of the brachial artery is palpable on the anterior aspect of the elbow, medial to the tendon of the biceps, and, with the use of a stethoscope and sphygmomanometer (blood pressure cuff) often used to measure the blood pressure.

The brachial artery is closely related to the median nerve; in proximal regions, the median nerve is immediately lateral to the brachial artery. Distally, the median nerve crosses the medial side of the brachial artery and lies anterior to the elbow joint.

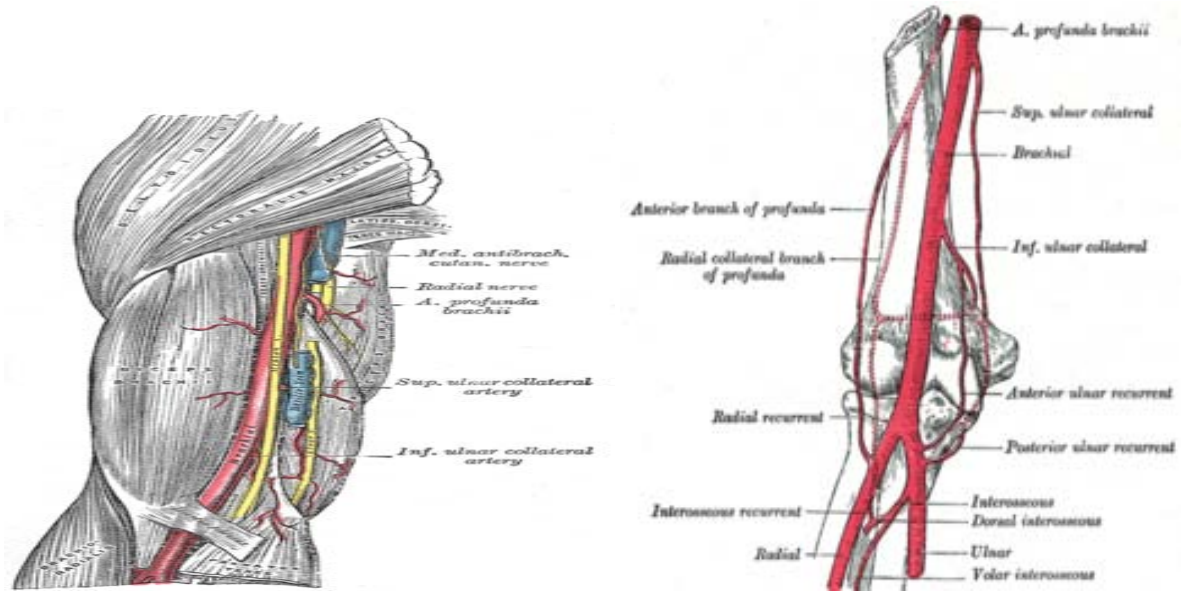

Fig 1.1: The anatomy of the Brachial Artery in Human Beings.

1.4 Immune complexes

Binding between antigen and antigen-specific antibody results in a reaction product which is an antigen-antibody complex or simply 'immune complex'. Immune complexes interact with many

cells of the immune system, causing activation or inactivation, and they might trigger the cytokine network. In the presence of plasma proteins, especially those belonging to the complement system, immune complexes will grow to more than strictly complexes between antigen and antibody. In fact, a number of different proteins have been identified as becoming fixed to immune complexes, thereby building up large protein constructions of which antigen and antibody are only a portion. The proteins found on immune complexes include the complement proteins C1q, C4b, C3b and factor H as well as anti-antibodies (rheumatoid factors, anti-idlotypes) and fibronectin. Both exogenous (foreign) and endogenous (self, autologous) antigens may trigger immune responses that result in the formation of immune complexes. Immune complexes are three-dimensional structures forming a lattice-type of sequence between antigens and antibodies with a ratio that may vary essentially according to the size of the antigen, the density of antigenic epitopes, and the isotype, subclass, poly/monoclonality and affinity of the antibody. The interaction between antigen and antibody does not result from chemical bonding bur rather is due to electrostatic forces. Therefore, the physicochemical properties of a given immune complex preparation are the result of a dynamic process between build-up and breakdown, contributing to constant variability of the characteristics of immune complexes in vivo. The immune complex structure is favored by the Y shaped configuration of the immunoglobulin molecules and by their abundance of water-repelling non polar groups known to favor auto aggregation of immunoglobulin M (IgM) or IgG in Solution.(Urs E Nydegger (1998)

1.5 Sizes of immune complexes

The size of immune complexes is believed to influence their biological activities, including their deposition and precise sites of tissue localization, as well as their removal by the monocyte-macrophage system, and their efficiency in activation of the serum complement pathways. Levinsky *et.al.* (1977) determined immune complex activity in sera from SLE (systemic lupus erythematosus) patients after the serum proteins had been fractionated according to size by gel chromatography. Based on a study of the sera from seven patients, immune complexes of intermediate size (1-1*5 x 106) were found in patients with renal involvement, while those of larger size (2 5-4 x 106) were associated with extra renal manifestations of SLE.

K. S. K. Tung *et.al*. (1981) determined that with regard to the molecular size of circulating immune complexes, the majority of patients studied were found to show both large- and small-sized complexes. Such a finding might be expected in any human disease state associated with a high prevalence of detectable circulating immune complexes.

R A Mageed *et.al.* (1991) worked on rheumatoid arthritis (RA) and studied in relation to different manifestations of the disease. Circulating immune complexes from the sera of 94 patients (50 with extra-articular disease) and 10 matched controls were fractionated by sucrose density gradient ultracentrifugation. The composition, immunoglobulin and rheumatoid factor (RF) concentrations within each of the fractions were determined by a sensitive enzyme linked Immunosorbent assay (ELISA). Intermediate size (14S-21S) IgG complexes containing RF activity and 22S IgG-IgM RF complexes were found in the sera of 40 patients with RA, while intermediate size complexes of self associated IgG kF and larger size complexes (>22S) of IgG RF and IgM RF were associated with extra-articular features of RA (50% of extra-articular disease). Complexes containing IgA were found in the sera of many patients with RA, and dimeric IgA RF mainly in patients with extra-articular disease. These results support the view that whereas small size circulating immune complexes are of no primary pathogenic importance in synovitis, large size (>22S) circulating immune complexes may play a role in extra-articular disease in RA. Current understanding of the formation of large complexes provides a biological explanation for their occurrence and effects.

1.6 Computational fluid dynamics

Computational fluid dynamics, usually abbreviated as CFD, is a branch of fluid mechanics that uses numerical methods and algorithms to solve and analyze problems that involve fluid flows. Computers are used to perform the calculations required to simulate the interaction of liquids and gases with surfaces defined by boundary conditions. The fundamental basis of almost all CFD problems is the Navier–Stokes equations, which define any single-phase fluid flow. These equations can be simplified by removing terms describing viscosity to yield the Euler equations. Further simplification, by removing terms describing vorticity yields the full potential equations. Finally, these equations can be linearized to yield the linearized potential equations.

(http://en.wikipedia.org/wiki/Computational_fluid_dynamics).

Because blood is a non-Newtonian fluid, its rheological properties depend on shear rate and the dimensions and geometry of the conduit through which it flows. Blood is a concentrated suspension of formed elements that includes erythrocytes (red blood cells (RBCs)), leukocytes (white blood cells (WBCs)), and platelets. RBCs are flexible, biconcave disks and constitute; 45% of blood by volume. Circulating WBCs are approximately spherical in shape with a diameter ;8–12 mm and are ;1000 times less abundant than RBCs. Platelets are discoid particles with a diameter ;2 mm, constituting ;1/800 of total cell volume. These cellular components are suspended in plasma, an aqueous solution that generally follows Newtonian dynamics. However, the two-phase nature of blood and the interactions between blood cells result in non-Newtonian dynamics, especially in the microcirculation where vessel dimensions become comparable to cell diameters (Popel and Johnson, 2005).

Computational Fluid Dynamics (CFD) is the art of replacing such PDE systems by a set of algebraic equations which can be solved using digital computers. Computational Fluid Dynamics (CFD) provides a qualitative (and sometimes even quantitative) prediction of fluid flows by means of mathematical modeling (partial differential equations), numerical methods (discretization and solution techniques), software tools (solvers, pre- and post processing utilities). CFD enables scientists and engineers to perform ‘numerical experiments’ (i.e. computer simulations) in a ‘virtual flow laboratory’. Numerical simulations of fluid flow (will) enable architects to design comfortable and safe living environments, designers of vehicles to improve the aerodynamic characteristics ,chemical engineers to maximize the yield from their equipment, petroleum engineers to devise optimal oil recovery strategies, surgeons to cure arterial diseases (computational hemodynamics), meteorologists to forecast the weather and warn of natural disasters, etc.

The results of a CFD simulation are never 100% reliable because the input data may involve too much guessing or imprecision, the mathematical model of the problem at hand may be inadequate, the accuracy of the results is limited by the available computing power.

1.7 CFD Software

"Fluent" is the general name for the collection of computational fluid dynamics(CFD) programs sold by Fluent, Inc. of Lebanon, NH. The Mechanical Engineering Department at Penn State has a site license for Fluent, along with its family of programs. Up to 20 users can run Fluent simultaneously in the Graduate Computing Lab.

- **Gambit** is the program used to generate the grid or mesh for the CFD solver.
- **Fluent** is the CFD solver which can handle both structured grids, i.e. rectangular grids with clearly defined node indices, and unstructured grids. Unstructured grids are generally of triangular nature, but can also be rectangular. In 3-D problems, unstructured grids can consist of tetrahedrals (pyramid shape), rectangular boxes, prisms, etc.
- Since version 5.0, Fluent can solve both incompressible and compressible flows.
- The normal procedure in any CFD problem is to first generate the grid (with Gambit), and then to run Fluent.
  (http://www.mne.psu.edu/cimbala/Learning/Fluent/gambit_introduction.htm)

Computational Fluid Dynamics (CFD) simulation of blood and air flow has been a subject of significant research effort. Over the last decade great progress has been made in computational modelling of blood flows to measure hemodynamic variables (L. Jou *et.al.* 2003, T. Hassan *et.al.* 2004).There have also been numerous studies of aerosol deposition in the respiratory system (Y., Zhang *et.al.* 2005) . However the application of these techniques to clinical evaluation of individual patients has been limited because it is very difficult to generate the accurate anatomic geometric models upon which the approaches depend. The theoretical and experimental studies are performed based on simplified or idealized models which are inconsistent with real situations.

Chapter 2 Review of Literature

2.1 Autoimmune Diseases

Auto immune diseases with the exception of rheumatoid arthritis and autoimmune thyroiditis, are individually rare, but together they affect approximately 5 percent of the population in Western countries. (Sinha AA *et.al.*1990, Jacobson DL *et.al.*1997).

Immune complexes are thought to play a part in the pathogenesis of synovitis and in the adverse immunological events of autoimmune diseases such as systemic lupus erythematosus and rheumatoid arthritis (RA). (McDougal J S *et.al.*1985, Korbet S M *et.al.*1984) Immune complexes have been demonstrated in synovial tissue, synovial neutrophils, synovial fluid, (Zvaifler N J 1974) and sera (Franklin E C *et.al.*1957) from patients with RA, and these findings have stimulated the development of numerous assay procedures for their measurement. In RA, the detection and measurement of circulating immune complexes has been seen as a potential laboratory guide to disease activity and as an indicator of impending or deteriorating extra-articular disease, though their pathological significance remains poorly understood. In experimental immune complex disease in animals the pathogenic effect of circulating immune complexes seemed to be dependent on their size and composition. (Cochrane C G. *et.al.* 1968).

In human systemic lupus erythematosus, the presence or absence of different sizes of circulating immune complexes has been found to correlate with different complications of disease, such as renal involvement,(Levinsky R J. *et.al.* 1977) though others disagree on the details of these findings.(Tung *et.al.* 1981). In RA synovial fluid immune complexes were found to be of both intermediate (6S-19S) and large (22S-30S) size and to consist of IgG bound to IgG rheumatoid factor (RF).(Stanworth D R *et.al.* 1977).

2.2 Immune complex

The size of immune complexes is believed to influence the biological activities, including their deposition and precise sites of tissue localization, as well as their removal by the monocyte-macrophage system, and their efficiency in activation of the serum complement pathways. Studies on the immune complex size in SLE patients, however, are limited. Levinsky *et.al* (1977) determined immune complex activity in sera from SLE patients after the serum proteins had been fractionated according to size by gel chromatography. Based on a study of the sera from seven patients, immune complexes of intermediate size (1-1*5 x 106) were found in patients with renal involvement, while those of larger size (2 5-4 x 106) were associated with extra renal manifestations of SLE. Tung *et.al.*(1981) determined the size of circulating immune complexes in the sera from a representative number of patients with different manifestations of SLE.

Ann Kari Lefvert *et.al*. (1995) tested one hundred patients who had survived a myocardial infarction before the age of 45 years and 90, age- and sex-matched healthy individuals were investigated for circulating immune complexes (CICs) and the presence of complement C4 null alleles (C4Q0). CICs were found in increased concentrations in 20% of patients and 6.7% of control subjects.

The estimated size of the immune complexes was 175 to 300 kD in 3 patients and in 1 control subject, between 300 and 900 kD in 15 patients and in 5 control subjects, and equal to or greater than 900 kD in 1 patient and in no control subjects. Eleven patients and 3 control subjects had a mixed pattern with complexes of different sizes. The concentration of plasma IgG, IgA, and IgM did not differ between patients and control subjects, nor was there any correlation between the amount of immunoglobulins and the amount of CICs. (Ann Kari Lefvert *et.al.*1995).

Deposition of immune complexes (IC) is considered to be an important pathogenetic mechanism in systemic lupus erythematosus (SLE) (Koffler, Schur & Kunkel, 1967; Krishnan & Kaplan, 1967). Granular deposits of immunoglobulins and complement components, presumptive evidence of IC, are frequently found in renal glomeruli, skin, choroid plexus and lung of patients with SLE. Recently, circulating IC have also been detected in over half of SLE patients based on several newly developed techniques (Theophilopoulos, Wilson & Dixon, 1976; Nydegger *et al.*,

1974; Eisenberg, Theophilopoulos & Dixon, 1977; Levinsky, Cameron & Soothill, 1977). These studies have, in general, demonstrated a correlation between immune complex levels and clinical disease activity though some exceptions have been recorded (Cano *et al.,* 1977*)*; some patients have also revealed an inverse relationship between disease activity and serum complement levels (Bardana *et al.,* 1973; Cameron *et al*., 1976).

2.3 Diagnosis of Autoimmune Diseases

The first step in managing patients with any disorder is proper diagnosis. Diagnosing autoimmune diseases can be particularly difficult, however, because these disorders can affect any organ or tissue in the body, and produce highly diverse clinical manifestations, depending on the site of autoimmune attack. Moreover, disease symptoms are often not apparent until the disease has reached a relatively advanced stage.

(NIH, 2005) Diagnosis of an autoimmune disease typically begins with a careful health history, including assessment of possible occupational and environmental exposures. Many of the early symptoms of these disorders, such as fatigue, joint and muscle pain, fever, or weight change, is nonspecific. While these symptoms alone may not point to a particular autoimmune disease, when considered in retrospect they can help to pinpoint when the disease process began. Added diagnostic clues may be revealed through family history, as the presence of autoimmune disease in a patient's family further suggests that an autoimmune disease should be considered among the diagnostic possibilities. Similarly, a social and occupational history may identify exposures associated with a particular autoimmune disorder.

Laboratory testing helps to establish the location and extent of disease. Such testing can reveal the presence of specific autoantibodies, which can be a strong indicator of an autoimmune disorder. Although laboratory testing has limitations, it is currently the cornerstone of diagnosis. Some immunologic tests are difficult to interpret, however, and must always be considered along with clinical findings. Recent studies suggest that autoantibody detection may be valuable in earlier diagnosis of autoimmune diseases, thereby allowing treatment to be initiated sooner. Research has shown that individuals who go on to develop clinical manifestations of type 1 diabetes, for example, often have had multiple antibodies to the insulin-producing islet cells for

some time before disease is evident. The presence of such antibodies, especially if coupled with a family history and genetic factors associated with the disease, increases the likelihood that symptoms will appear in the future. In some instances it may be possible to use antibodies to monitor response to treatment or to forecast an exacerbation of a disease in remission. However, because some autoimmune diseases are caused by infiltrating cells rather than autoantibodies, practical tests for cell-mediated autoimmune reactions are a high priority need.

Imaging technology can also be a valuable diagnostic tool. For example, imaging tests that reveal areas of demyelination in the brain (plaques) have been useful for diagnosing and staging multiple sclerosis and for monitoring responses to therapy. Other specialized imaging technologies are of increasing value in following the course of several autoimmune disorders.

The absence of generally accepted diagnostic standards has hampered efforts of researchers and clinicians to identify autoimmune diseases at early stages. For a few diseases, including lupus, multiple sclerosis, and rheumatoid arthritis, professional groups have developed diagnostic criteria. These criteria are essential for epidemiologic studies, but may not always be valid for clinical diagnosis in individual cases. Because so many early symptoms of autoimmune disease are relatively non-specific, years may go by before a definitive diagnosis can be reached and treatment initiated. These long delays represent a particular hardship for patients, who too often go from one physician to another seeking a cause of their illness. These problems have stimulated recent investigations seeking better objective indicators of disease called biomarkers. Often based on a particular pattern of biochemical and immunologic data linked to a specific disease or disease risk, biomarkers have the potential to considerably improve our ability to diagnose autoimmune disorders earlier in the disease process.

2.4 Treatment of Autoimmune Diseases

(NIH, 2005) Treatments to reduce the symptoms of most autoimmune diseases are available, but definitive cures have yet to be developed. In general, two approaches to treatment are currently available. The first involves replacing or repairing impaired function. For example, patients with type 1 diabetes mellitus can take insulin to replace the hormone that is not produced by their damaged pancreatic islet cells. Similarly, patients with autoimmune thyroiditis can be treated

with thyroid hormones. These methods do not arrest the autoimmune process, although the patient may undergo remission while receiving symptom-based treatment. In most cases, however, the patient must depend on replacement therapy throughout his or her lifetime.

Sometimes a damaged organ can be replaced by transplantation. For example, scientists are now testing the effectiveness of islet cell transplant as a treatment for diabetes. Patients with end-stage renal disease or dilated cardiomyopathy may be candidates for a kidney or heart transplant. In the future, stem cell therapies might allow replacement or repair of damaged organs. Replacement therapy is most likely to be successful if the impaired function is localized to a single organ system.

The second treatment approach centers on suppressing the destructive autoimmune response. Systemic autoimmune diseases often require general suppression of the immune response. Immunosuppressive drugs reduce the overall immune response and thereby ameliorate the manifestations of the disease. However, because these drugs also reduce the individual's resistance to infection, they must be used with great caution. In addition, they often have adverse side effects. Such treatments are most often used in debilitating diseases such as lupus and rheumatoid arthritis.

Much effort has been devoted in recent years to developing more focused therapies than global immune suppression, most of which target a specific step in the tissue-damaging inflammatory response. A number of promising new biologic agents that produce more targeted immunosuppression are already in advanced clinical trials. They include monoclonal antibodies that decrease T cells or B cells specifically, act on only activated T cells, inhibit particular cytokine mediators of inflammation, or block the recruitment and localization of lymphocytes to the target organ. Although these targeted approaches usually have fewer side effects, they may increase the patient's vulnerability to infection, and therefore also must be used with caution. Moreover, a therapy that benefits one autoimmune disease will sometimes make another disorder worse.

2.5 Morphology of Brachial Artery

The brachial artery, a continuation of the axillary, begins at the distal (inferior) border of the tendon of teres major and ends about a centimeter distal to the elbow joint (at the level of the neck of the radius) by dividing into radial and ulnar arteries. At first it is medial to the humerus, but gradually spirals anterior to it until it lies midway between the humeral epicondyles. Its pulsation can be felt throughout divide the course of brachial artery in 3 equal parts i.e. proximal 1/3, middle 1/3 and distal 1/3. It lies successively on 3 muscles (from above downwards - long head of triceps, coracobrachialis and brachialis), is in contact with 3 important nerves (Radial, ulnar and median), associated with 3 veins (2 Venae comitans and 1 basilic vein) and gives 3 main branches (profunda, superior et inferior ulnarcollaterals). The average length of brachial artery is 26.29 cm and diameter is 0.442cm (Patnaik ,2002) the average length of radial artery is 17cm and diameter is 0.264cm (Buxton (1998)), the average length of ulnar artery is 14.5cm and diameter is 0.25 cm (Buxton ,1998).

2.6 Computational Fluid Dynamics

Now these immune complexes when circulate in the body, it may show some change in blood pressure, velocity, viscosity and other parameters which can be used for prognosis of any immune disease. These simulation studies regarding the flow properties were done using the Computational Fluid Dynamics. Many of the simulation studies regarding the flow properties of blood were done by many of the scientists like as C.C. Botar *et.al.* 2010, studied the Validation of CFD simulation results in case of portal vein blood flow.

The fundamental basis of almost all CFD problems is the Navier–Stokes equations, which define any single-phase fluid flow. These equations can be simplified by removing terms describing viscosity to yield the Euler equations. Further simplification, by removing terms describing vorticity yields the full potential equations. Finally, these equations can be linearized to yield the linearized potential equations. Historically, methods were first developed to solve the Linearized Potential equations. Two-dimensional methods, using conformal transformations of the flow about a cylinder to the flow about an airfoil were developed in the 1930s. (Milne-Thomson, L.M. (1973).

The computer power available, paced development of three-dimensional methods. The first paper on a practical three-dimensional method to solve the linearized potential equations was published by John Hess and A.M.O. Smith of Douglas Aircraft in 1967 (Hess, J.L.; A.M.O. Smith (1967)).

The recent development of computational fluid dynamics (CFD) technology now allows complex numerical simulation of the cardiovascular system. A few computational studies have been made of steady and unsteady blood flow in the human aortic arch (Shahcheraghi *et.al.*(2002), Morris L *et.al.*(2005)). In those studies that have been undertaken, CFD analyses have been used to evaluate specific parameters, such as the velocity distribution of blood flow in the aorta, wall pressure, and wall shear stress on the aortic wall, which are very difficult to measure in vivo. Using CFD technology, we performed a three-dimensional (3D) numerical simulation of blood flow from an arterial cannula during cardiopulmonary bypass within a model of the human aortic arch.

Because the CFD analysis of the complex geometry of the aorta required multiple complex processes, we have only been able to perform the simulation using one representative case to date. Creating an appropriate geometric model and computational grids suitable for CFD analysis was an especially cumbersome and very time-consuming process as these processes have not yet been automated. The technique shows promise and, once the processes are automated in the future, it may be possible to simulate every patient's vascular geometry before an operation in order to predict blood flow patterns and assess the risks associated with different cannulation methods. It is possible that this could reduce the risk of stroke significantly. A similar approach has been tried in other fields of surgery (Castro MA *et.al.* 2006).

Cardiovascular diseases (CVDs) are being considered as a main public health problems in the world. By mean of Ansys Fluent CFD® software, the research reports of the blood flow computational simulation in zones affected by stenosis were reported. Different severity of stenosis, based on variation of 36%, 51% and 80% reduction of lumen, and considering concentric and eccentric plaques, were simulated. The models were implemented considering

steady state flow, using the k-e turbulence model. Simplifying, the blood was assumed as Newtonian fluid with μ= 0.0036 Pa·s and ρ =1050 Kg/m3, and arteries were treated as a rigid cylindrical model, with geometric approach to a representative model of the affected zones of the arterial tree, as carotid, coronary, renal, and femoral vessels. With the purpose to define a representative lesion, a medical image reconstruction of a chronic coronary artery stenosis was made. The Navier-Stokes equations were used to solve the fluid flow problems with CFD analysis through numerical methods. The results of simulation of different percentage of stenosis, with significant increases in velocity, Reynolds number, and wall shear stress; meanwhile the pressure decreases, due to energy conversion. As the degree of stenosis increases, phenomenon of recirculation and turbulence flow can be generated.(S. Echavarría *et.al.* 2011).

The blood flow complex characteristics have been investigated along the time through simulations based on mathematical models that include constitutive equations describing the hemodynamics and its relations with the deformable vessels wall. The computational techniques applied to model the blood flow in the circulatory system have been used to investigate either the velocity field or the pressure field. The vessel walls have been treated as rigid (Perktold K, Rappitsch G (1995)) ones or considering significantly simplified or reduced geometries for the deformable wall models (Cairncross RA *et.al*. (2000)). The approximation of rigid walls was made mostly due to the difficulty of solving the coupled blood flow/vessel deformation problem and was justified by the observation that, under normal conditions, wall deformability does not significantly alter the velocity field (Cairncross RA *et.al*.(2000)). Modeling the three dimensional blood flow in compliant vessels is extremely challenging for a number of additional reasons such as: geometry acquisition, accurate constitutive description of the behavior and induced movement of the tissue, inflow and outflow boundary conditions, etc. The vessel wall, due to its elasticity, changes shape in response to flow field dynamics and surrounding organs movement. Thus, the homodynamics is inherently a fluid–structure interaction phenomenon, which supplementary requires knowledge about the flow rate time evolution. When simulating venous regions the flow rate time dependency is reduced and the flow regime could be considered in steady state. Therefore, the most realistic methods, for hemodynamics description in veins, as in this case, are the real fluid – structure interaction ones (Vierendeels JA *et.al.* 2000;

Watanabe H *et.al*.2002). In these methods the geometry is modeled by conventional Finite Element Method (FEM) and the fluid flow by CFD technique.

Due to its capability the CFD technique have been mostly used for studying the complex behavior of the blood flow. The first CFD studies (Finnigan P *et.al.* 1990; Taylor CA *et.al.* 1998) used idealized geometries to calculate the blood flow characteristics and properties like wall shear stress and residence time. Later, due to the development of medical imaging techniques, more accurate and realistic geometries (Perktold K *et.al*. 1991) have been used in blood flow simulation studies.

2.7 Particulate Nature of Blood

Because blood is a non-Newtonian fluid, its rheological properties depend on shear rate and the dimensions and geometry of the conduit through which it flows. Blood is a concentrated suspension of formed elements that includes erythrocytes (red blood cells (RBCs)), leukocytes (white blood cells (WBCs)), and platelets. RBCs are flexible, biconcave disks and constitute 45% of blood by volume. Circulating WBCs are approximately spherical in shape with a diameter of 8–12 mm and are 1000 times less abundant than RBCs. Platelets are discoid particles with a diameter of 2 mm, constituting 1/800 of total cell volume. These cellular components are suspended in plasma, an aqueous solution that generally follows Newtonian dynamics. However, the two-phase nature of blood and the interactions between blood cells result in non-Newtonian dynamics, especially in the microcirculation where vessel dimensions become comparable to cell diameters (Popel and Johnson, 2005).

For Newtonian laminar flow through a circular cylindrical tube, the Hagen-Poiseuille solution describes the pressure drop per length:

Dp=DL ¼ 8mQ=pr4.

where Dp is the pressure drop in length DL, m is the viscosity of the fluid, r is the radius of the tube, and Q is the volume rate of flow. For a non-Newtonian fluid such as blood, this equation

does not apply, but we can still measure the Dp/DL and Q and calculate an apparent viscosity, mapp:

mapp ¼ ðDp=DLÞpr4=8Q:

If m0 denotes the viscosity of the plasma, then the ratio mapp/m0 is defined as relative viscosity, and is denoted by mrel. Apparent and relative viscosities are not intrinsic properties of the blood: both vary with hematocrit, RBC aggregation state, and vessel geometry. Apparent viscosity can be measured in any flow in which the Newtonian solution is known. Above given two equations and relative viscosity can be extended to any flow system; if its structural geometry and elasticity are unknown we need only measure flow and pressure with and without blood cells to calculate the relative viscosity. It is not only the red blood cells that determine the flow characteristics of blood. White blood cells, despite their relatively low number compared to RBCs, contribute dramatically to organ blood flow resistance. Helmke *et al*.(1997) observed that at constant arterial flow rate, arterial pressure was increased significantly when relatively few leukocytes were added to a suspension containing erythrocytes at physiological hematocrits. We assess the effects of RBC concentration and conduit size on blood flow and quantify the additional resistance contributed by flowing, rolling, and firmly adhering leukocytes. Using this approach, we can reproduce the Fahraeus and Fahraeus- Lindqvist effects by explicitly accounting for the particulate nature of blood. This represents a first step toward achieving a fundamental understanding of the complex fluid dynamics of blood.(Chenghai Sun and Lance L. Munn 2005).

2.8 Blood Flow Modeling

The flow model considers the thixotropic characteristics of the blood. In a non- Newtonian fluid, as in the blood case, the relation between the shear stress and the strain rate is nonlinear, and can be even time-dependent; therefore a ratio between shear stress and strain rate (or shear-dependent viscosity) has been defined. Moreover, this concept is more useful for fluids without time-dependent behavior, as in the case of portal vein circulation.

The computational modeling of the blood flow has been done considering three dimensional incompressible Navier-Stokes equations written in a strong conservation form for mass and momentum. Finding the solution of the governing equations is difficult using traditional analytical techniques, especially for such a complicated system, which involves 3D irregular geometry, complex fluid-structure interaction and non-Newtonian viscosity. Numerical techniques have been required, hence the need for CFD. The CFD software used for simulations was the ANSYS's FLUENT. The model implemented to describe the hemodynamics was the Reynolds stress model (RSM), which is the most elaborate turbulence model that FLUENT software provides. The RSM model is abandoning the isotropic eddy-viscosity hypothesis, and closes the Reynolds-averaged Navier-Stokes equations by solving transport equations for Reynolds stresses together with an equation for the dissipation rate. Since the RSM accounts for effects of streamline curvature, swirl, rotation, and rapid changes in strain rate, in a more rigorous manner than the one-equation and the two equation flow models, it has been used in simulation due to its greater potential to give accurate predictions for complex flows [FLUENT 6.3.26 user guide].

A steady state model has been used; the reduced time dependency of the blood flow in portal vein system has been neglected. The differential equations have been discretized in a manner of finite element method. The operation and the boundary conditions have been specified. The vessel wall has been treated as elastic. A dynamic mesh model has been used in order to address the movement of the mesh in the steady state solver. The no-slip condition has been imposed, meaning that the speed of the fluid relative to the boundary is 0, but at some distance from the boundary the flow speed must equal that of the fluid bulk. The blood viscosity has been defined according to the non-Newtonian power law (C.C. Botar *et.al*. 2010).

2.9 Computational Models of Blood flow in Arteries

In the past four decades, much of the research has been concentrated on the relationship between blood flow in arteries and, the sites where atherosclerosis develops (Berger & Jou, 2000). The aorta divides into a number of arteries, which in turn divide again into smaller arteries. These

smaller arteries break up to give rise to capillaries , which form a capillary bed the preferable site for manifestation of atherosclerosis (O'Brien & Ehrlich, 1977). Herein are presented some main studies and the most relevant achievements that depict the advances that have taken place in this field. The first attempt to model the blood flow in normal blood vessels has been mapped back to 1950s. The equation of viscous motion for laminar flow of a Newtonian and incompressible fluid was analyzed by Womersley (1955) in an infinitely long and straight circular pipe. The main issue was to calculate the velocity and flow rate in arteries according to the pressure gradients measured by McDonald (1955). The velocity profiles were calculated by representing the physiological pressure as a Fourier series. The major simplifications made in this study were: the assumption of a rigid circular tube to represent large arteries and the assumption of a periodic pressure gradient only function of time, whereas it is generated by a pulse wave of finite velocity. In 1957, the same author included wall motion as equation for a thin, uniform and linearly elastic wall in the model to improve these limitations. Womersley's analysis was useful to gain a general understanding of the relevant forces involved in arteries flow (Ku, 1997). O'Brien and Ehrlich gave an idealized model of the trifurcation flow in renal arteries in 1977. Renal arteries are bilateral side branches that form a trifurcation branch with the abdominal aorta. They assumed the geometry to be two-dimensional and straight-sided, instead of curved and three-dimensional. The model, despite of being a very simplified one was able to show the complexity of the unsteady flow patterns at a trifurcation and the relation to the development of atherosclerosis. After comparing steady and unsteady results, it was found that the WSS and recirculation were highly related and time-dependent through the cardiac cycle. The finite-difference calculations presented in this study may not be quantitatively highly accurate but they seem to present a very valid qualitative tendency of flow patterns. This study remained confined at two-dimensional level due to the limited computational resources. Certain features of the flow, such as secondary motions and circumferential variations of shear stress, features that may be critical to atherogenesis and plaque growth were not taken into account. In 1980, Avolio modeled human arterial system using the linear form of the Navier-Stokes equations. A multi-branched model of the human arterial system with 128 segments was constructed based on anatomical branching structure. The arterial segments were represented by uniform elastic tubes

and characterized by electrical transmission-line properties. Avolio's model was much an improvement over the previous electrical analogue models but it has been demonstrated that the complete blood flow patterns, such as secondary motion, cannot be obtained with a simpler 1D method.

Till recently, the computational models used to predict blood flow were restricted to one or two dimensions. The increased computational hardware capability helped to create three-dimensional models, which had an enormous impact on the understanding of vascular hemodynamics since the problem could be described more properly than using 1D and 2D methods. Perktold & Rappitsch (1995) described the regions where separation and recirculation are expected to occur in a carotid artery bifurcation. The used time-dependent, three-dimensional, incompressible Navier-Stokes equations for non-Newtonian fluids for simulations. A shear model was used to approximate the complex rheological behaviour of blood. In this model, the apparent viscosity was expressed as a function of the shear rate.

In this investigation, the effect of the distensible artery wall was also included and it was described as a coupled fluid-structure interaction because of the coupling of fluid motion and the wall motion. The velocity profiles, WSS distribution and the zones of reversed flow were calculated throughout the cardiac cycle. These results were compared with the results of another study in which an independent ring model was used, and it was found that the coupled fluid-structure was more realistic and having influence on the flow dynamics. However, a relation between the results and atherogenesis couldnot be established. After this, Rappitsch & Perktold (1996) proposed a numerical analysis for an axisymmetric domain in order to study the influence of the flow patterns, such as WSS and reversed flow, on the mass transport.

Till 1996, there were no studies involving the direct comparison between MRI (Magnetic Resonance Imaging) measurements and numerical simulation, but Steinman *et al*. (1996) showed good concurrence between measurements of blood velocity profiles obtained by MRI and numerical simulations. This study was significant in stating the validity of numerical modelling in giving an accurate solution that can easily match MRI *in vivo* results. Taylor *et al*. (1998a,

1998b) qualitatively and quantitatively assessed the blood flow filed in abdominal aorta using the finite element method. The velocity profiles were obtained under two conditions namely resting and exercise. In resting conditions, a recirculation zone was formed along the posterior wall of the aorta, immediately distal to the renal vessels. In these areas low values of time-averaged WSS were present and these areas are hypothesized to be more vulnerable to cholesterol accumulation and atherogenesis. Under moderate exercise conditions, all regions of low WSS and high oscillatory shear index were eliminated. This proved that exercise is an important means of increasing blood flow and thereby preventing atherosclerosis (Taylor *et al*., 2002). Shipkowitz *et al*. (1998, 2000) and Lee & Chen (2002, 2003) also developed numerical procedures based on finite volume method to simulate the flow in the abdominal aorta and its peripheral branches but by using a slightly different approach. Shipkowitz *et al*. (1998) compared the influence of assuming an axial uniform or a fully developed axial velocity profile in the inlet boundary condition and reported similar results for both. Lee & Chen (2002, 2003) demonstrated that a steady inflow may fairly describe the time-averaged blood flow behavior when compared with a corresponding pulsatile case. Carneiro *et al*. (2008a) evaluated whether the upstream branches in the abdominal aorta lead to more complex flow patterns downstream. Studies of blood flow have been conducted since a long time but realistic studies and models have become possible only in the last decade. CFD simulations of blood flows necessitate the accurate reconstruction of geometry via imaging techniques like Computed tomography (CT) or MRI.

A method for detailed evaluation of vessel anatomy and flow rate was developed by Cebral *et al*. (2002) using MRI angiographic data. More recently, Kagadis *et al*. (2008) and Nanduri *et al*. (2009) used cardiovascular models reconstructed from CT scan to carryout CFD simulations. These models can describe blood flow in patient specific models in a non-invasive manner and thus can be very important in medical interventions. In models, laminar flow depicted blood flow in healthy vessels and turbulence during the cardiac cycle depicted the presence of vascular diseases. He & Jackson (2000), in their studies on fundamental aspects of turbulence dynamics, observed that turbulence intensity is attenuated in accelerating phases and increased in decelerating phases of the cardiac cycle, mainly associated with the radial propagation of

turbulence. Numerical analysis of turbulent flow in stenosed pipes has also been performed so as to predict which turbulence model could be more suitable in predicting flow profiles in stenosis region. In such an investigation ,carried out by Varghese & Frankel (2003) pulsatile turbulent flow in a rigid wall stenosed tube was simulated. The objective of their study was to predict the flow features downstream of a stenoses under both steady and pulsatile conditions through direct numerical simulations. The findings of this study were that the acceleration of the fluid through the stenosis resulted in WSS magnitudes that exceeded upstream levels, but WSS levels accompanied the flow separation zones that formed immediately downstream of the stenosis. A simulation model that included fluid-structure interaction (FSI) and a turbulence model with realistic boundary conditions in a vessel with different degrees of stenoses were developed by Li *et al*. (2007). To achieve this objective, a coupled simulation process was performed using two commercial packages, Fluent and Abaqus, for flow modeling and wall deforming calculation, respectively. This study showed that severe degree of stenosis causes a higher pressure drop across the vessel constriction, resulting in both higher blood velocities and peak WSS. One more important observation of this study revealed the intimate correlation that exists between the increase of stenosis degree and the characteristics of the wall vessel displacement. The inclusion of vessel wall displacement mechanisms in stenosis progression and consequent atherosclerotic plaque rupture allowed for a better numerical analysis.

2.10 Investigating the flow field in arteries

Fluid mechanics modeling can be approached experimentally, theoretically, or numerically. Fluids experiments are restricted by physical limitations (e.g., equipment, measurements) and instrumentation; however, in flow experiments complex geometries can be modeled, and complex physics phenomena (e.g., turbulence) potentially have better representation in *in vitro* experiments than in the other two approaches. In theoretical models, equations governing the system are defined. Simplifying assumptions on the physical nature of the situation are made to construct a solvable problem, often limiting this approach to simple systems (geometrically and

physically); however, broad understanding is conveyed in a concise, mathematical form. Computational fluid dynamics (CFD) modeling often entails assumptions on the nature of the problem in order to solve the equations defining the problem, but complicated geometries can be accommodated. Numerical models are primarily limited by computational resources and by the understanding of the physical nature of the problem (Tannehill *et al.*, 1997). In numerical modeling, decisions on the modeling parameters (e.g., fluid properties, boundary conditions) potentially impact the simulation quality. Reducing the model complexity can result in reduced solution time; however, the speed increase must be balanced against the cost to the quality of solution. Two long disputed simplifications in artery models (both *in vitro* and numerical) are discussed here: the Newtonian fluid assumption and the use of compliant walls. Blood is a multiphase fluid, with the primary particle constituent being red blood cells. A shear-thinning fluid, blood becomes decidedly non-Newtonian when flowing through small vessels where the size of red blood cells is on scale with the vessel (Ku, 1997). However, in large arteries shear rates are sufficiently high and the length scale is large enough to approximate blood as a Newtonian fluid (Caro *et al.*, 1978; Strony *et al.*, 1993). In both an experimental and a numerical model of low Reynolds number flow in an averaged carotid bifurcation, Gijsen *et al.*, (1999), found differences in axial velocity profiles and in the prevalence of secondary flow for different viscosity models. Further, they found that slight differences in shear rate control the effect of Newtonian flow on the velocity distribution, accounting for discrepancy between findings of the influence of the Newtonian fluid assumption. Using the classification system proposed by Tang *et al.,* (2004), implementing the assumption that flow in arteries is Newtonian in nature is on the lowest order, Level III, of impact of the simplification on computational results. Differing opinions also exist on the importance of modeling arterial flow with compliant or rigid walls. Real arteries are tethered *in situ*; hence, there are small axial deformations, but there are appreciable circumferential changes with pressure. Comparisons between geometrically identical, compliant and rigid models of a large scale averaged human carotid bifurcation with the same flow waveform illuminate differences of wall motion, mean wall shear stress, peak wall shear stress, and separation points (Anayiotos *et al.*, 1994; Anayiotos, 1990), but the authors suggest that these differences are not major. Although Perktold *et al.,* (1994), concluded that

compliance was not as important hemodynamically as differences in individual geometries, they reported flow recirculation regions and peak wall shear stress values were altered by the consideration of compliance in the model. A geometric approximation of the Balasubramanian model (Balasubramanian, 1980) was reproduced and modeled under both rigid and compliant boundary conditions (Reuderink, 1991). Reuderink reported that wall deformation correlated with cross-sectional lumen area and that the compliant model demonstrated smaller recirculation regions and lower wall shear stresses near peak systole than the rigid model. Further, the numerically simulated reverse flow region developed at the deceleration of the flow waveform, contrary to the reports that describe the development of the recirculation region as forming just prior to peak systole (e.g., Perktold *et al.*, 1994; Reuderink, 1991). The explanation of Reuderink for the time of reversed flow development is given as a pseudo-capacitance of the compliant model. As the flow accelerates the model distends and higher velocities are seen in the distal internal carotid. As the flow decelerates flow separation occurs at the sinus (Reuderink, 1991).

Using a geometry based on the reports of Ku *et al.*, (1985) but employing an alternative pressure wave form, Perktold and Rappitsch (1995) reported differences between compliant and rigid wall models. The bulk flow patterns were consistent between the two models, but quantitatively they showed differences. Along the internal carotid during the acceleration phase of systole, the compliant model showed lower axial flow velocity than the rigid model (when the vessel expands); however, during the deceleration phase, the compliant model showed higher axial velocity than the rigid model (when the compliant vessel contracts). The compliant model has smaller recirculation regions, a lower magnitude of negative axial velocity, and smaller secondary velocities. At the side wall flow separation is greater in the distensible model, with a longer reversed flow region length, but at the outer sinus wall the separation region is smaller in the compliant model than in the rigid model. For some periods of the pulsatile cycle, reversed flow is only seen in the rigid model. Further, the compliant model showed lower wall shear stress values than the rigid model, especially at the divider wall of the internal carotid artery near the bifurcation region. Maximum displacement occurs in the bifurcation region at the side wall, which happens to be a zone of low principal stress at the inner surface of the wall, and normal displacements are much greater than tangential displacements. Again referring to the

classification by Tang *et al.,* (2004), the effect of solid mechanics inclusion with fluid mechanics models is a Level II factor, indicating much greater influence on the result than considering non-Newtonian behavior.

Petkova *et.al*. (2003) examined blood flow in a model of the portal vein with and without obstructions to simulate conditions, which are common in liver diseases. They evaluated the impact of both conditions on the flow behaviour and found significant differences in the two models. Blockages, even when the flow conditions did not change, had an impact on the velocity magnitude, pressure, strain rate and shear stress in a model of portal vein hypertension due to liver diseases.

C.C. Botar *et al.* validated the CFD simulation results in case of portal vein blood flow. The blood flow complex characteristics have been investigated along the time through simulations based on mathematical models that include constitutive equations describing the hemodynamics and its relations with the deformable vessels wall. The computational techniques applied to model the blood flow in the circulatory system have been used to investigate either the velocity field or the pressure field. Yoshiyuki Tokuda *et.al*. studied three-dimensional numerical simulation of blood flow in the aorticarch during cardiopulmonary bypass. This study confirmed that blood flow during cardiopulmonary bypass can be simulated and visualized. Computational fluid dynamics could be applied in the future to assess an individual's risk of stroke.

S. Echavarría *et.al* performed CFD Analysis of Blood Flow in Arteries with Stenosis and illustrated the usefulness of computational techniques in the field of bioengineering as a noninvasive alternative for comprehension of the behavior of blood flow in certain vascular pathologies like stenosis. S. M. Abdul Khader *et.al*. studied effect of increased severity in patient specific stenosis of common carotid artery using CFD and found that velocity increases in throat region with the increase in severity. Due to the eccentric constriction, the flow behavior changes abruptly in the downstream of the stenosis. There are no significant changes in proximal side during early systole for the various severity cases. During peak systole, the flow increases at the throat region forming a jet and later disrupts suddenly forming eddies due to pressure drop in

downstream side. (Patnaik ,2002) The brachial artery, a continuation of the axillary, begins at the distal (inferior) border of the tendon of teres major and ends about a centimeter distal to the elbow joint (at the level of the neck of the radius) by dividing into radial and ulnar arteries. The brachial artery was a continuation of axillary artery at lower border of teres major and bifurcating into radial and ulnar arteries at a mean distance of 2.99 cm (ranging from 1.0 to 4.5 cm) below intercondylar line, its total length being on an average 26.29 cm (ranging from 20.5 to 29.0 cm). Buxton (1998) , Venkatanarasimha (2007) the total length of radial and ulnar arteries being on an average 17cm and 14.5 cm respectively.

These lengths are used by Nicole varble *et.al*.in their work on Computational Fluid Dynamic Model of Arteriovenous Fistula Anastomosis to Study the Effects of Vessel Size and Pressure Gradient on the Presence of Clinical Steal and a Thrill. From this study they concluded the result of three aims, first is to create the geometry based on the average blood vessel diameter, length and boundary conditions. Analyze the entrance to the access vessel and the magnitude and direction of flow to the hand, other is to change the boundary conditions to that of a hypertensive patient (elevated blood pressure). Determine flow conditions at the access changed, and last is that if backwards flow does not occur in 1st then to determine the boundary conditions at the outlet for which backwards flow occurs. If backwards flow does occur, determine a threshold at which this does occur and quantify in terms of differential pressure between the two outlets.

Chapter 3 Methodology

In order to understand the change in blood pressure in the brachial artery, this study will employ computational fluid dynamics (CFD) to simulate blood flow. CFD requires information about the geometry to be simulated, which in the current case will be obtained from human brachial artery.

3.1 Geometry, Material Properties, Boundary Conditions and Assumptions

Assumptions include: Non- pulsatile flow, blood vessels are idealized as perfect cylinders with sections of constant diameter, diameters are based on the average size of blood vessels complied from the current literature, inlet and outlet pressures and flows are based on average pressures and flows in the vessels and blood, the working fluid, is considered a non-Newtonian fluid with an average density and viscosity .

Because this project focuses only on the entrance of the brachial artery, the entirety of the arm vasculature will not be modeled. The area modeled will include a portion of the brachial artery before and after the bifurcation , and a portion of the radial and the ulnar arteries. All fluid will enter the system at the proximal brachial artery (closer to the center of the body), and will flow through the radial and ulnar artery after passing bifurcation. At the inlet a velocity boundary condition will exist and at the two exits a mass flow outlet will exist. The model was created in 2D in order to analyze the pressure change across the brachial artery. Figure 1 below shows a 2D schematic of the geometry including labeled boundary conditions.

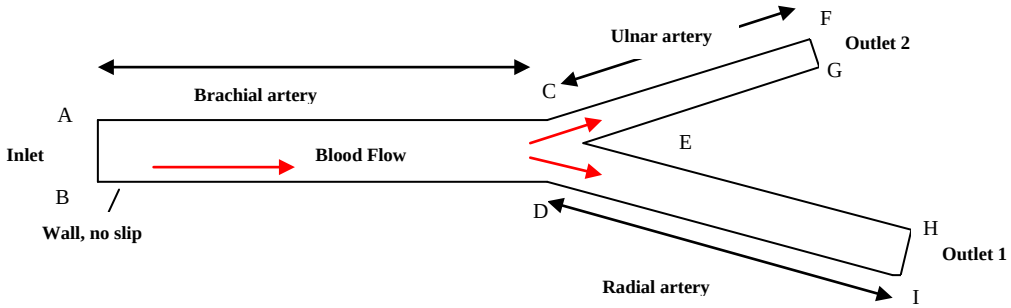

Fig 3.1: 2D schematic of modeled blood vessel geometry and boundary conditions.

Table 3.1: Geometry and Boundary conditions.

Name	Value	Units	Citation
Brachial Artery Diameter	0.442	cm	Patnaik(2002)
Radial Artery Diameter	0.264	cm	Buxton(1998)
Ulnar Artery Diameter	0.25	cm	Buxton(1998)
Brachial Artery Length	26.29	cm	Patnaik(2002)
Radial Artery Length	17	cm	Buxton(1998)
Ulnar Artery length	14.5	cm	Buxton(1998)

3.2 Geometry Development

Gambit

Gambit is used to construct the flow geometry, along with the mesh for solving the equations of motion and continuity at fixed points.

3.2.1 Points Creation in Gambit

Table 3.2: Coordinates of the geometry

	Point	Coordinates
Inlet	A	0, 26.29
	B	0.442, 26.29
	C	0,0
	D	0.442, 0
Point Of Bifurcation	E	0.214, -0.072
Outlet2	F	-7.25, -14.5
	G	-7, -14.5
Outlet1	H	8.678, -17
	I	8.942, -17

The boundary conditions were applied in Gambit. Using the Fluent 5/6 solver, a velocity inlet and two outlet vents were established. The exact values of these outlet mass flow rates and velocities will be set once the mesh is imported into Fluent

3.2.2 Lines creation in Gambit

After opening gambit a large black screen with a Cartesian coordinate system is appeared and the values of various coordinates was entered .After creating points with various coordinates these points are now joined to form the edges of geometry .

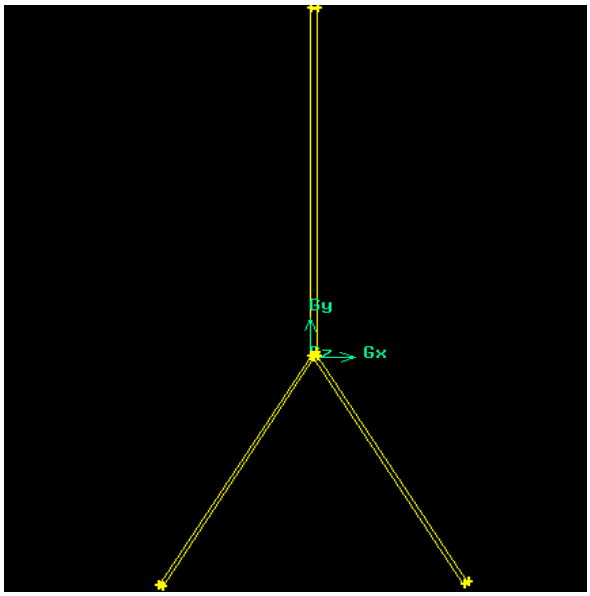

Fig 3.2: Geometry after joining the co-ordinates .

3.2.3 Face creation

After joining the points , faces were created using the command of face creation and various edges are are labeled according to the zone creation . Edge 1 is labeled as inlet , Edge 2 is labeled as oulet1 , Edge 3 is labeled as oulet 2, and other edges as wall.

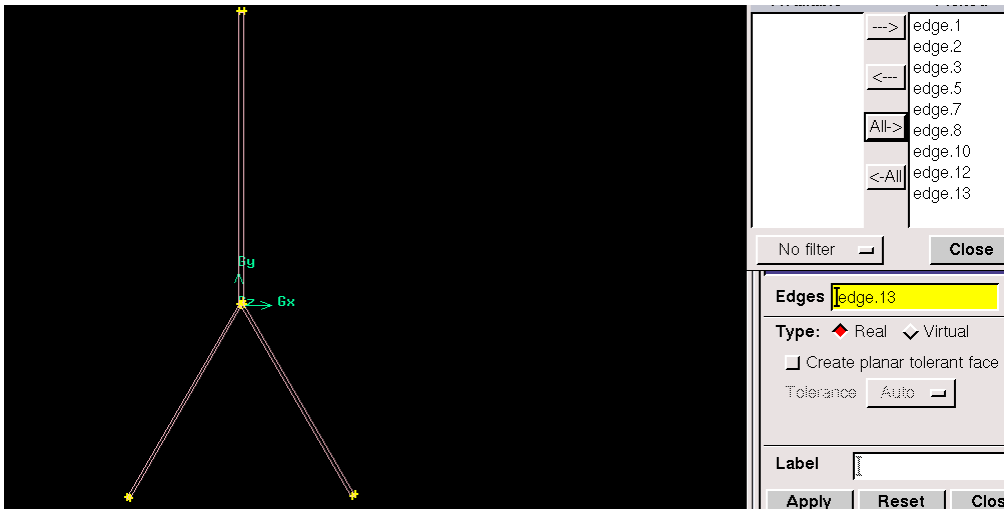

Fig 3.3: Face creation in the geometry.

3.2.4: Zone creation

After facing the zones were created to specify the geometry in wall, velocity inlet, outlet vent.

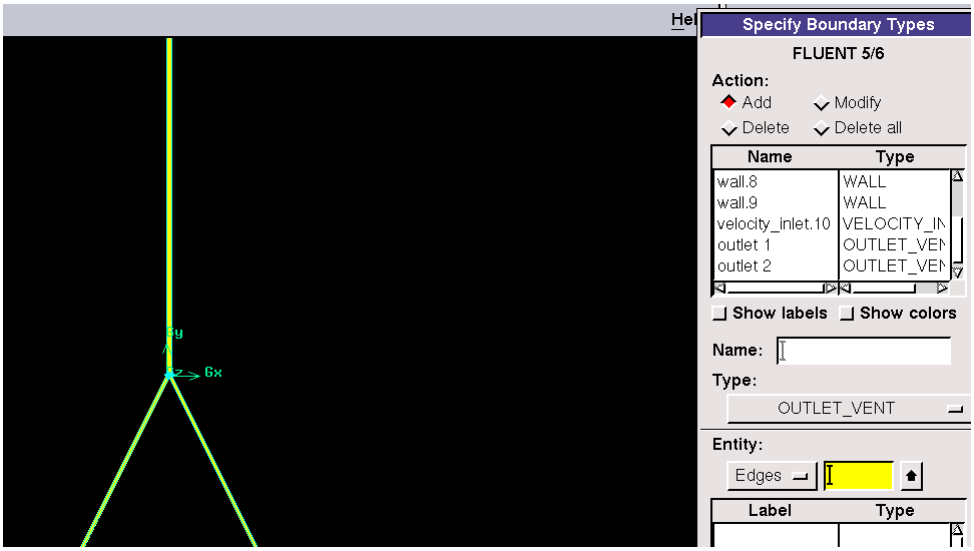

Fig 3.4: Zone creation in the geometry.

3.3: Meshing

Meshing was done after creating faces. Each face was meshed using the quad/ pave scheme with the interval size and spacing of 0.01 . As clear from the figure the meshing was finer in the middle and everywhere accept at the bifurcation and at the outlets .

The 195050 quadrilateral cells were created after meshing and 383909 mixed interior faces were there. The speed of meshing will depends upon the processor and the RAM of the computer used.

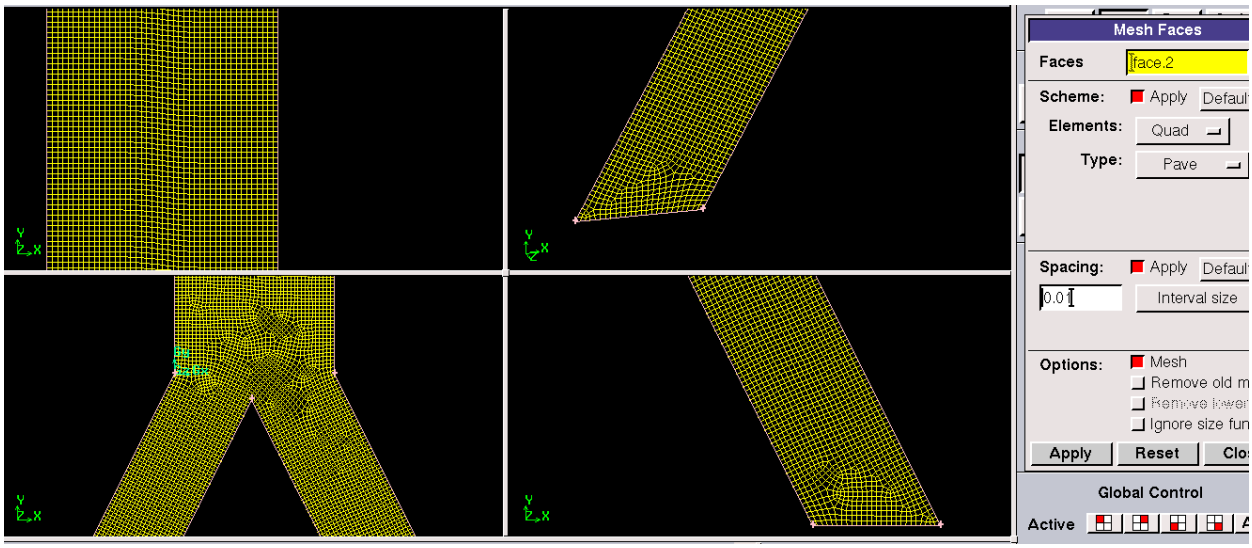

Fig 3.5: Geometry after meshing in four quadrants.

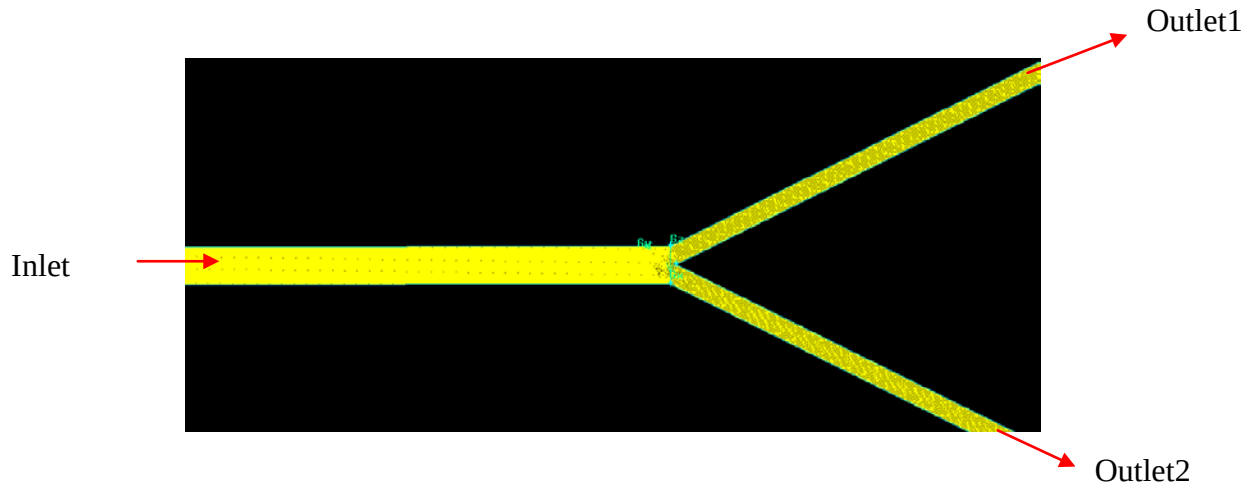

Fig 3.6: Geometry after meshing.

After meshing the geometry was exported to file name artery.msh and now this was imported for simulation in Fluent 6.2.16.

3.4: Fluid under conditions development in fluent and simulation of parameters

The geometry was developed in 2D, so the fluent was used in 2D run. After defining the mesh and unit systems for the problem, the geometry case was imported in .msh extension and grid checking was done to confirm that the geometry was properly imported or not. Importing was followed by scaling of geometry, as used for this project scaling was done in centimeters. The scaling was done only once for the import of geometry, the reported values of the Domain Extents will be reported in the default SI Unit of centimeters; the next step was to define the models that were to be used for the simulation. First, the solver model was chosen. In Fluent, the solver model can be chosen to be either pressure based or density based. The density model is typically used only for problems involving compressible flow, while the pressure based model is used for the majority of simulations. Since one of the assumptions for this problem was that the density of blood was constant throughout the geometry, the pressure based model was selected. Within the solver based model it was also necessary to define how the model varies with time; in other words whether it is steady or unsteady. For the first series of simulations, the steady state model was selected. The final determinations that needed to be made were whether or not the energy equation was to be used, and what type of viscous model was to be selected. Because there was no heat transfer or work being performed, the energy model was not used. The steady state model was run each flow rate and it was run using the k-epsilon turbulence model.

After defining the models that were to be implemented in running the simulations, the next step was to define the material properties that would be used. The default material was air with standard properties at room temperature. These default properties were changed to the properties of blood. At this time, it was necessary to define the boundary conditions to serve as a basis for the computations that would be used to analyze the problem. No heat transfer was defined passing through the artery. After defining the boundary conditions, the system had all the data necessary to begin running the simulation. The first step in running the simulation was to define the boundary conditions from the inlet of the artery as the basis for the computations. Next,

Convergence criteria were set to specify how accurate the results should be. In this case, convergence criteria were set at the level of E-05, which typically gives good convergence without requiring excessive computation times. Finally, the computations were performed. This was achieved by specifying the number of iterations that needed to be performed. Typically, about 2,000 iterations were specified, and the solution would converge within the first few hundred iterations. After the necessary iterations were performed, it was possible to analyze the results. Contours and vector plots were then drawn over the length of artery to get an idea of the physical properties over different locations within the geometry, most notably the velocity fields, pressure distribution.

3.4.1: Case 1

The study of brachial artery under normal conditions .The solver used for this was steady 1^{st} order implicit with k-epsilon (2equation) model. The normal blood flow parameters used are, blood density 1060 kg/m^3 , viscosity 0.005 kg/ms, pressure at inlet 17198.59 Pascal and pressure at outlet1 and outlet2 are 8932.598 Pascal and 10265.82 respectively , convergence criteria used is 1e-05 and no. of iterations used were 1500 and solution converged at 1267 time step.

3.4.2: Case 2

The Study of variation of pressure along the length under normal conditions using the parameters of velocity inlet and outlet pressure was performed using the same k-epsilon(2 equation) model. The parameters for normal blood were taken and velocity at inlet 0.625m/s and outlet pressures i.e. outlet1 and outlet2 were 8932.598 Pascal and 10265.82 respectively.

3.4.3: Case 3

Multiphasic flow in the artery was tried to simulate with the solver steady 1^{st} order implicit k-epsilon model. In multiphasic flow the volume of fluid was used and 2 phases was selected. The material for one phase is blood and for other phase is immune complex. The normal parameter

used for blood are, blood density 1060 kg/m^3, viscosity 0.005kg/ms and for the other phase the density of particles used is 3200 kg/m^3. But the problem came with the putting the values in the parameters. In multiphasic mixture the inlet button for the velocity inlet is active but at the outlet the mass flow outlet was not applicable in the case. So the results were not recorded as desired because the available defendable parameters i.e. velocity inlet and mass flow outlet are not inserted in the model. So the idea to flow in multiphase was dropped and switched on to the combined density of the fluid by adding the density of extra flow during diseased condition and flow density of normal condition with the discrete phase flow of the immune complexes with trapping and escape in diseases.

3.4.4: Case 4

The change in pressure drop in brachial artery under systemic lupus erythematosus simulation condition was studied with the control parameters of the normal individuals and parameters of the diseased individuals. The solver used for this was steady 1st order implicit with k-epsilon (2equation) model. The blood velocity, viscosity, density for control are 0.625m/s, 1060 kg/m^3 ,0.005 kg/ms respectively and the immune complex were injected from the inlet surface and the diameter is calculated by using the values in the formula and taking the average diameter 1.223e-05 m .The values of all the parameters in the formula are used from the literature. In boundary conditions the inlet velocity and outlet vent with flow rates are used to calculate the change in pressure across the length of Brachial Artery.

$$D = \sqrt{\frac{18 \times v \times V}{g \times (d_p - d_m)}}$$

D = Diameter Of a Particle V = Terminal Velocity

v = Viscosity Of Medium g = Acceleration Of Gravity

d_p = Density Of Particle d_m = Density Of Medium

The immune complexes were inserted in the discrete phase with flow rate given in the table below. The material which was used to simulate the immune complex was inert calcium oxide as the density of the particle of the immune complex is near or less as compared with the density of the calcium oxide particle , the density is calculated from the same formula above.

In the diseased state the velocity is considered same as in the inlet in the control state but the density and viscosity were changed as the amount of the circulating immune complex and antibodies level in the blood increases upto a significant level. The values of density and viscosity in diseased persons were averaged to 1080 kg/m^3 , 0.0065 kg/ms respectively.

Table 3.4: Boundary conditions for Systemic Lupus Erythematosus

Systemic lupus Erythematosus			
Mass flow rate	Outlet1	Outlet2	Immune complex Injection
Control	0.00517214 kg/s	0.0048978 kg/s	6e-09 kg/s
Diseased	0.005186746 kg/s	0.00491169 kg/s	2.84998e-05 kg/s
Citation: Cano *et.al*. 1977, Tung *et.al*. 1980			

The velocity of immune complex injection was taken as 0.6m/s and start and stop time in one flow was between 0 to 20 seconds. The convergence criteria used for the flow was 1e-05 and the fluid was iterated for 2000 iterations in both the control and diseased case. The solution converged with in 6 hrs in both conditions.

3.4.5: Case 5

The change in pressure drop in brachial artery under glomerulonephritis simulation condition was studied with the control parameters of the normal individuals and parameters of the diseased individuals. The solver used for this was unsteady 1st order implicit with k-epsilon (2equation) model. The blood velocity, viscosity, density for control is 0.625m/s, 1060-1070 kg/m^3,

0.005 kg/ms respectively and the immune complex were injected from the inlet surface and the diameter is calculated by using the values in the formula 1 and taking the average diameter 1.223e-05 m. The operating conditions are default and in boundary conditions the inlet velocity and outlet vent with flow rates are used to calculate the change in pressure across the length of brachial artery. The immune complexes were inserted in the discrete phase with flow rate given in the table below. The discrete phase is used in trapping mode as the immune complexes in the glomerulonephritis are deposited inside the membranes .The material which was used to simulate the immune complex was inert calcium oxide as the density of the particle of the immune complex is near or less as compared with the density of the calcium oxide particle, the density is calculated from the same formula above.

In the diseased state the velocity is considered same as in the inlet in the control state but the density and viscosity were changed as the amount of the circulating immune complex and antibodies level in the blood increases and immune complex deposits are increased upto a significant level. The values of density and viscosity in patients with glomerulonephritis were averaged to 1100 kg/m^3, 0.007-0.0075 kg/ms respectively.

Table 3.5: Boundary conditions for Glomerulonephritis

Glomerulonephritis			
Mass flow rate	Outlet1	Outlet2	Immune complex Injection
Normal low	0.0060642 kg/s	0.0057426147 kg/s	0.000125399 kg/s
Normal mid	0.006480780826 kg/s	0.006137102174 kg/s	0.000250798 kg/s
Normal high	0.0071404689 kg/s	0.0067650175 kg/s	0.0003761977 kg/s
Patient 1	0.01060628 kg/s	0.010100644 kg/s	0.0001899886 kg/s
Patient 2	0.007849926269 kg/s	0.00743364173 kg/s	0.00032299807 kg/s
Patient 3	0.00715119533 kg/s	0.006141120669 kg/s	0.00005319968 kg/s
Citation: Valentino *et.al*. 1959			

The velocity of immune complex injection was taken as 0.6m/s and start and stop time in one flow was between 0 to 20 seconds. The convergence criteria used for the flow was 1e-05 and the fluid was iterated for 150 time steps with 20 iterations in one time step in both the control and diseased case. The solution converged with in 6 hrs in all the conditions. The conditions in this case are used with control was taken as the mean of the values of normal low, mid and high and the patients with varying values of immune complexes.

3.4.6: Case 6

The change in pressure drop in brachial artery under rheumatoid arthritis simulation condition was studied with the control parameters of the normal individuals and parameters of the diseased individuals. The solver used for this was steady 1^{st} order implicit with k-epsilon (2equation) model. The blood velocity, viscosity, density for control are 0.625m/s, 1060 kg/m^3 (as there is no significant flow of immune complex in control so the density is same as normal average), 0.005kg/ms respectively and the immune complex were injected from the inlet surface and the diameter is calculated by using the values in the formula and taking the average diameter 1.223e-05 m. The operating conditions are default and in boundary conditions the inlet velocity and outlet vent with flow rates are used to calculate the change in pressure across the length of brachial artery. The immune complexes were inserted in the discrete phase with flow rate given in the table below. The material which was used to simulate the immune complex was inert calcium oxide as the density of the particle of the immune complex is near or less as compared with the density of the calcium oxide particle; the density is calculated from the same formula above.

In the diseased state the velocity is considered same as in the inlet in the control state but the density and viscosity were changed as the amount of the circulating immune complex and antibodies level in the blood increases upto a significant level. The values of density and viscosity in diseased persons with articular and extra articular diseases were averaged to 1080 kg/m^3, 0.0065 kg/ms respectively.

Table 3.6: Boundary conditions for Rheumatoid Arthritis.

Rheumatoid Arthritis			
Mass flow rate	Outlet1	Outlet2	Immune complex Injection
Control	0.006382218 kg/s	0.006043767 kg/s	6.8e-10 kg/s
Patients with Articular	0.006803816 kg/s	0.006443007 kg/s	3.85697e-06 kg/s
Patients with Extra Articular	0.0072765 kg/s	0.006890627 kg/s	3.11596e-05 kg/s
Citation: Mageed *et.al*. 1991			

The velocity of immune complex injection was taken as 0.6m/sand start and stop time in one flow was between 0 to 20 seconds. The convergence criteria used for the flow was 1e-05 and the fluid was iterated for 100 time steps with 20 iterations in one time step in both the control and diseased case. The solution converged with in 6 hrs in all the conditions**.**

Chapter 4 Results

Computational fluid dynamics with the available parameters from the literature was performed. The simulations of blood flow in the brachial artery for normal condition and the disease condition for the respective diseases were performed and the pressure and velocity contours were analyzed. In each case the pressure profile contours were examined at inlet and outlets. The total pressure loss was calculated among inlet and outlets. The magnitude of total pressure change was calculated. The pressure contour plot was examined to determine which branch acts as a low pressure vessel and the direction the fluid will preferentially flow. And the velocity vector plot was examined to determine the direction of flow.

4.1: Case1

Initially, the brachial artery was simulated with normal conditions of outlet pressure and velocity to determine the flow conditions in the artery, the pattern and direction of flow was determined. The flow is straight and there is no reversal in the flow. Drop across the length was determined. Below is an image of the pressure change across the brachial artery with the simulated conditions in case 1 of the flow.

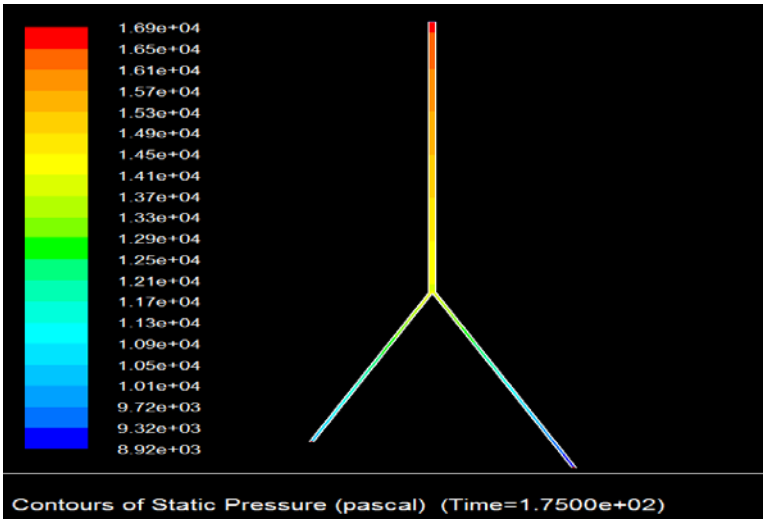

(a)

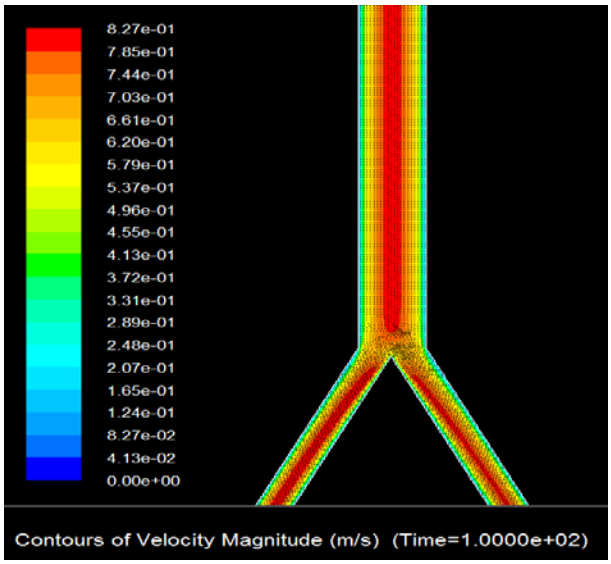

(b)

Fig 4.1: Contours of Static pressure (a) and Vectors of the velocity distribution (b) across the length of brachial artery.

By analyzing the contours of pressure and velocity profiles, it is clear that the pressure drop in the artery is maximum due to the bifurcation in it. The velocity contours are showing the increase in velocity across the length due to drop in pressure and this value is maximum at the bifurcation.

Table 4.1: Mass Weighted Average Surface integrals of flow were shown

Case 1	
Velocity Default Interior	1.0816 m/s
Inlet Velocity	0.9975 m/s
Velocity at Outlet1	1.1108 m/s
Velocity at Outlet2	0.9589 m/s
Net Velocity at Outlet	1.0426 m/s
wall shear Stress at inlet	2.75 Pascal
wall shear stress interior	0.4479 Pascal
wall shear stress outlet	0.925 Pascal

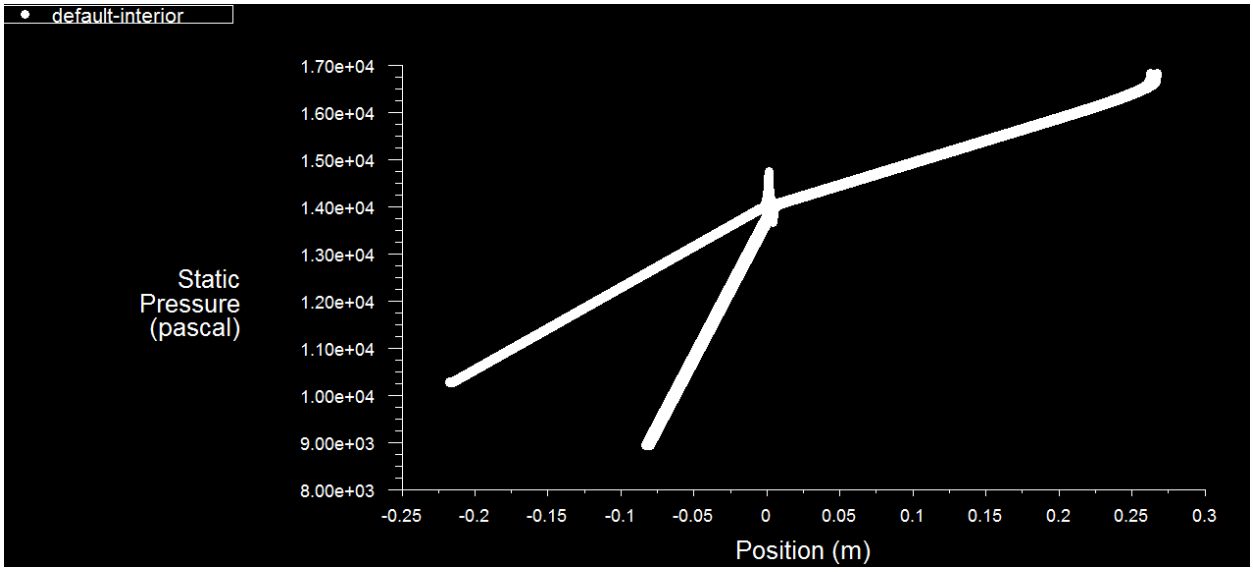

Fig 4.2: xy plot of Static Pressure in case1.

The above table is showing the surface integral mass weighted average values of steady flow of blood in the brachial artery. The xy plot of the static pressure is showing the variation of the pressure at different points.

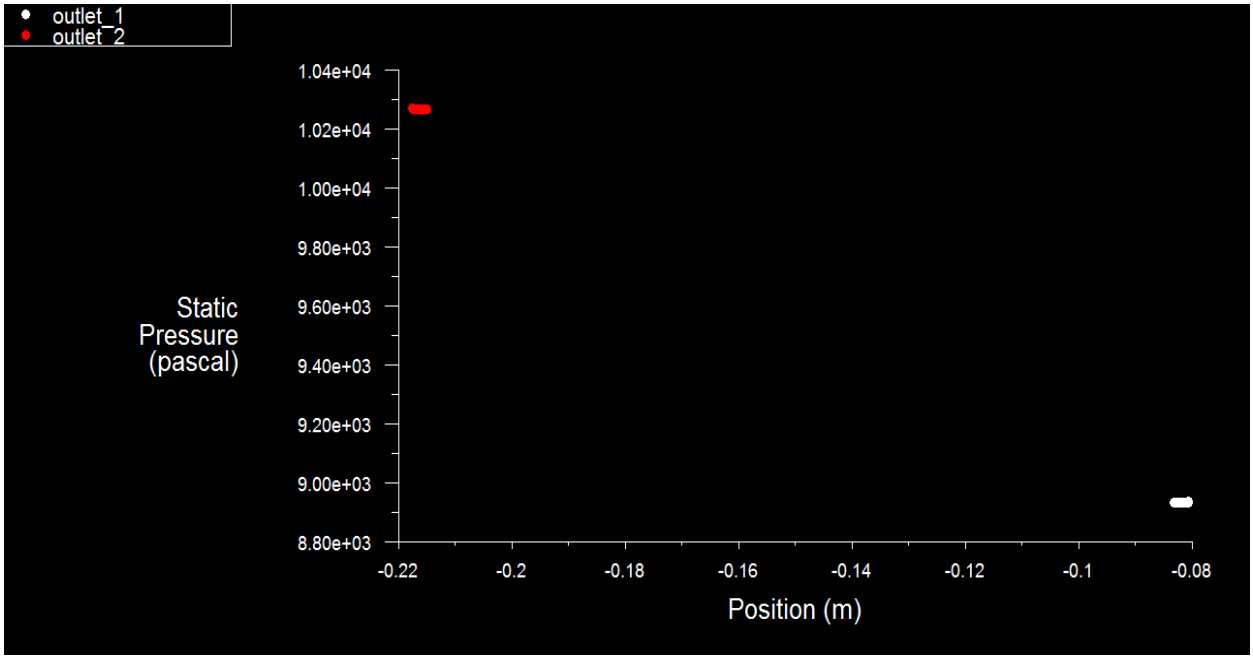

Fig 4.3: xy plot of Static Pressure in case 1 at outlet1 and 2.

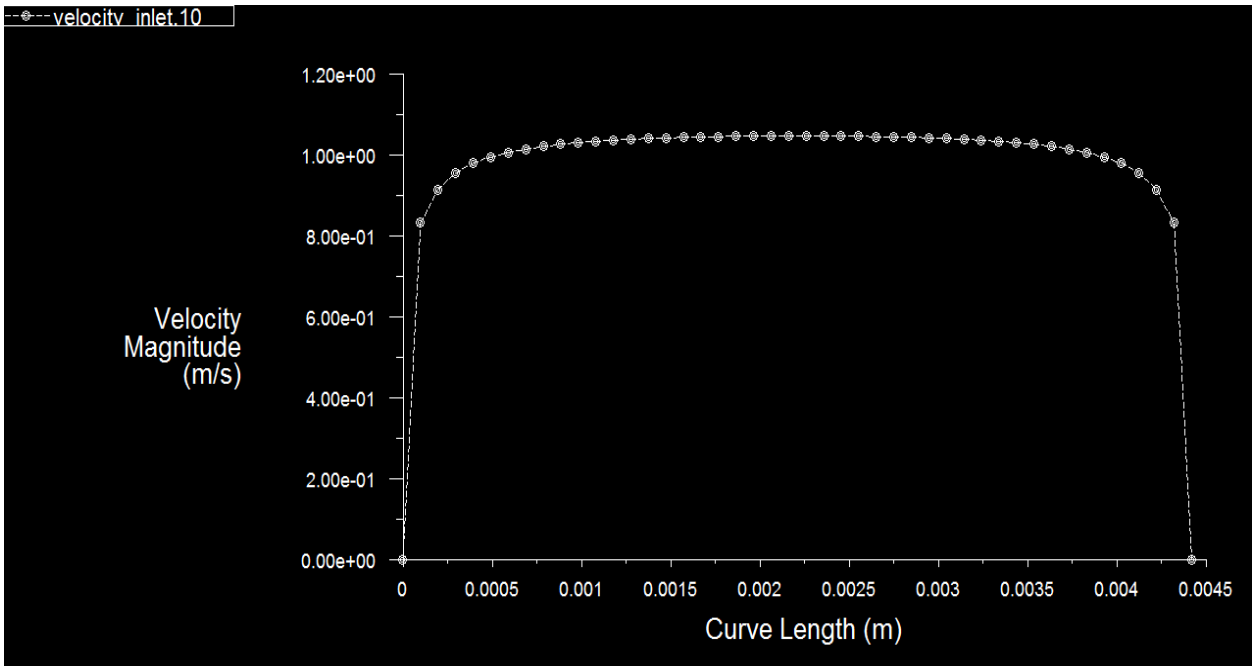

Fig 4.4: Curve length of velocity magnitude at inlet in case1.

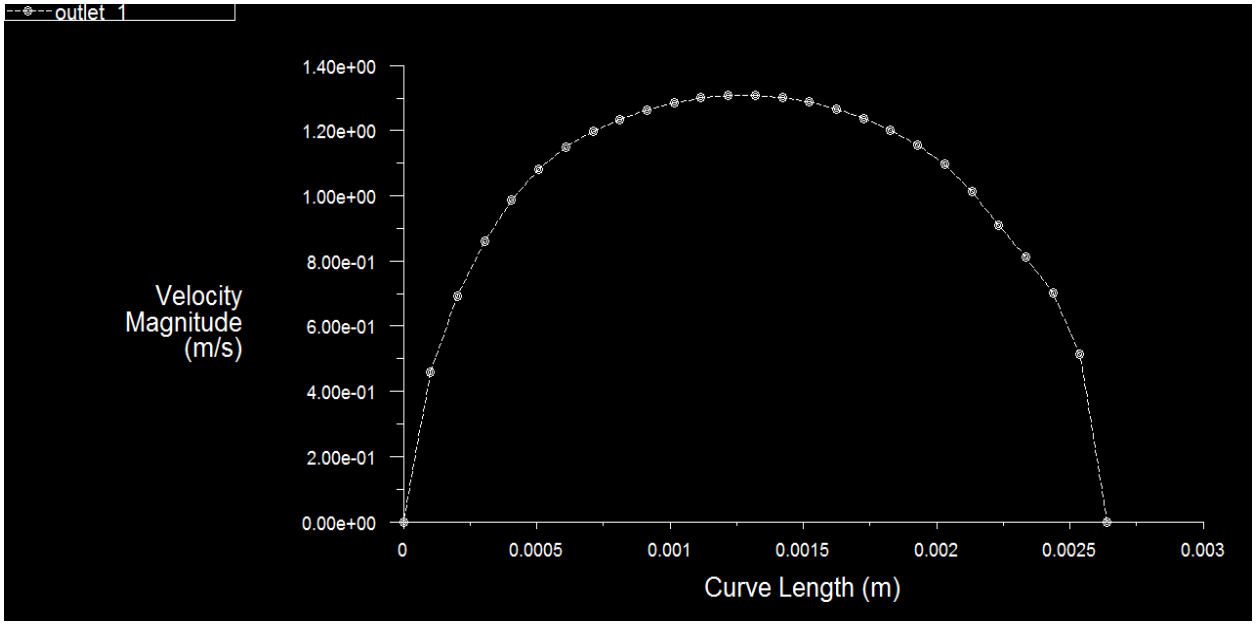

Fig 4.5: Curve length of velocity magnitude at outlet1 in case 1.

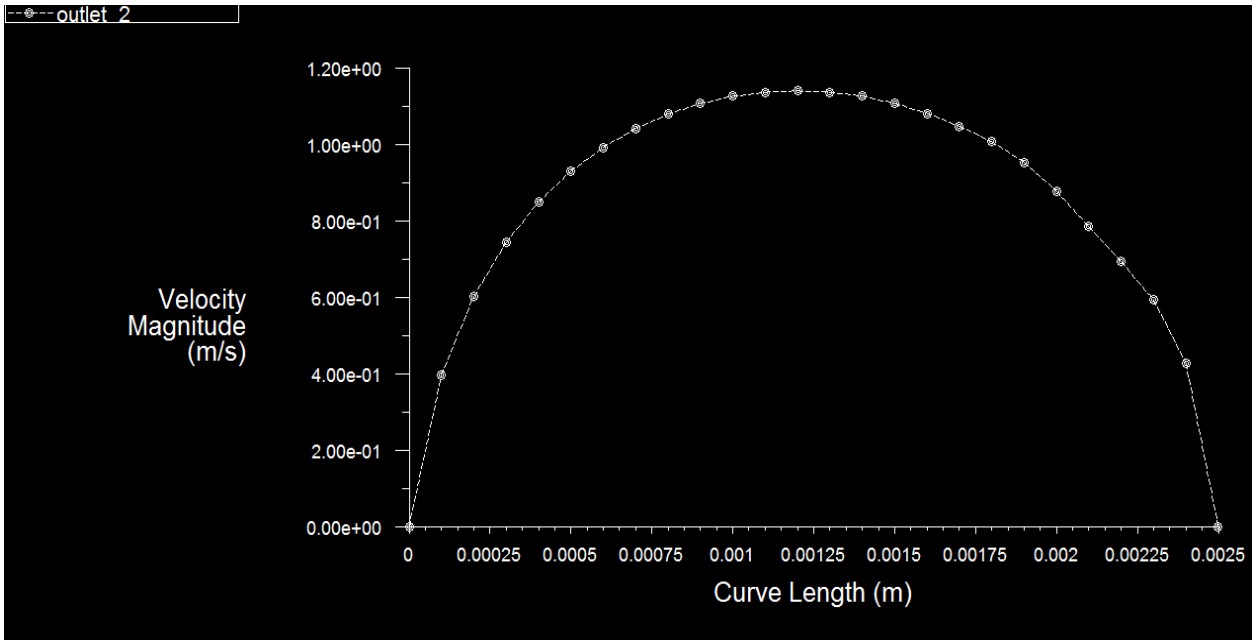

Fig 4.6: Curve length of velocity magnitude at outlet 2 in case 1.

Fig 4.3 is showing the difference in pressure between the two outlets and difference is due to the different diameter of the outlets, velocity at outlet 1 is more than the velocity at outlet 2, simulating the same condition in normal artery as documented in the literature. From Fig 4.3, 4.4, 4.5, 4.6 it is clear that the 1300 Pascal pressure difference at the two outlets leads to change in velocity of 0.20 m/s and the change in velocity at the inlet and outlet is due to the pressure drop between the inlet and outlets. The velocity magnitude is more at outlet1 implies that the pressure drop is more at outlet1 than at outlet2.

4.2: Case 2

In this case the pressure variation at the inlet and velocity change across the length was calculated with the available pressure at outlets and velocity inlet parameters.

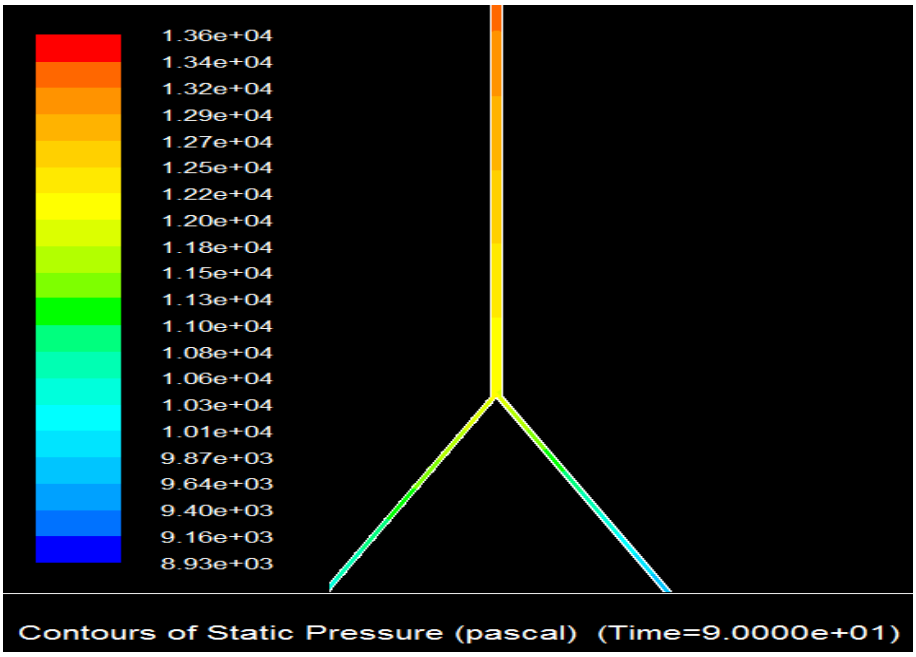

(a)

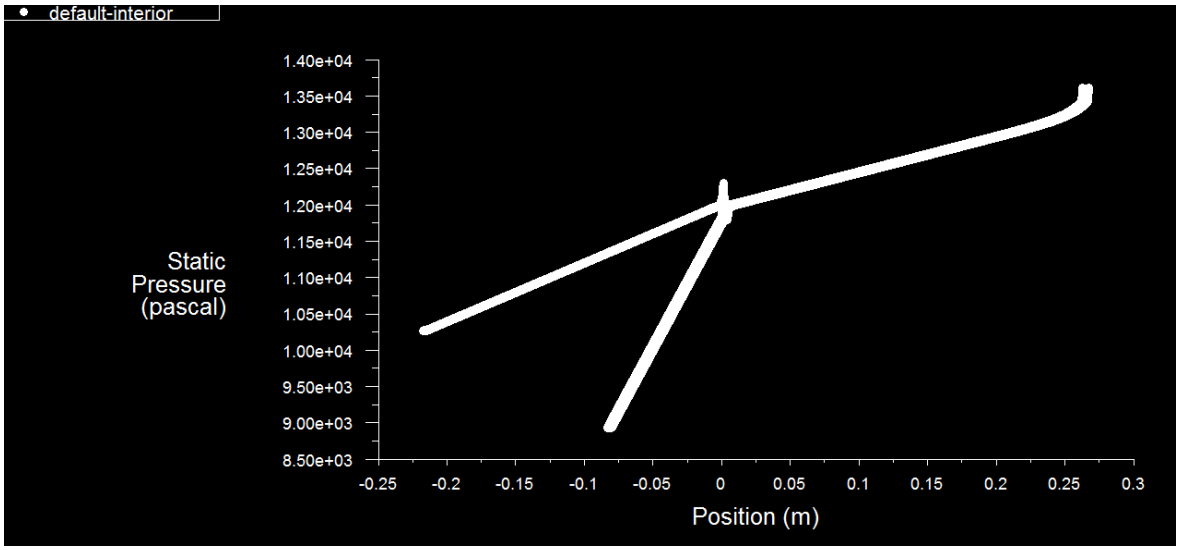

(b)

Fig 4.7: (a) Static Pressure contours of the case2, (b) xy plot of the Static Pressure.

As shown in Fig 4.7, the pressure contours and the variation of pressure along the length was measured at every point in the xy dimension of the artery.

Table 4.2: Mass Weighted Average surface integrals of flow

Case 2	
Pressure inlet	13651.78 Pascal
Interior pressure	12098.86 Pascal
Velocity interior	0.6868 m/s
Velocity outlet	0.6689 m/s
Wall shear stress inlet	2.775 Pascal
Wall shear stress interior	0.2175 Pascal
Wall shear stress outlet	0.434 Pascal

The above table is showing the mass weighted values of the surface integrals across the length of the brachial artery in the case 2.

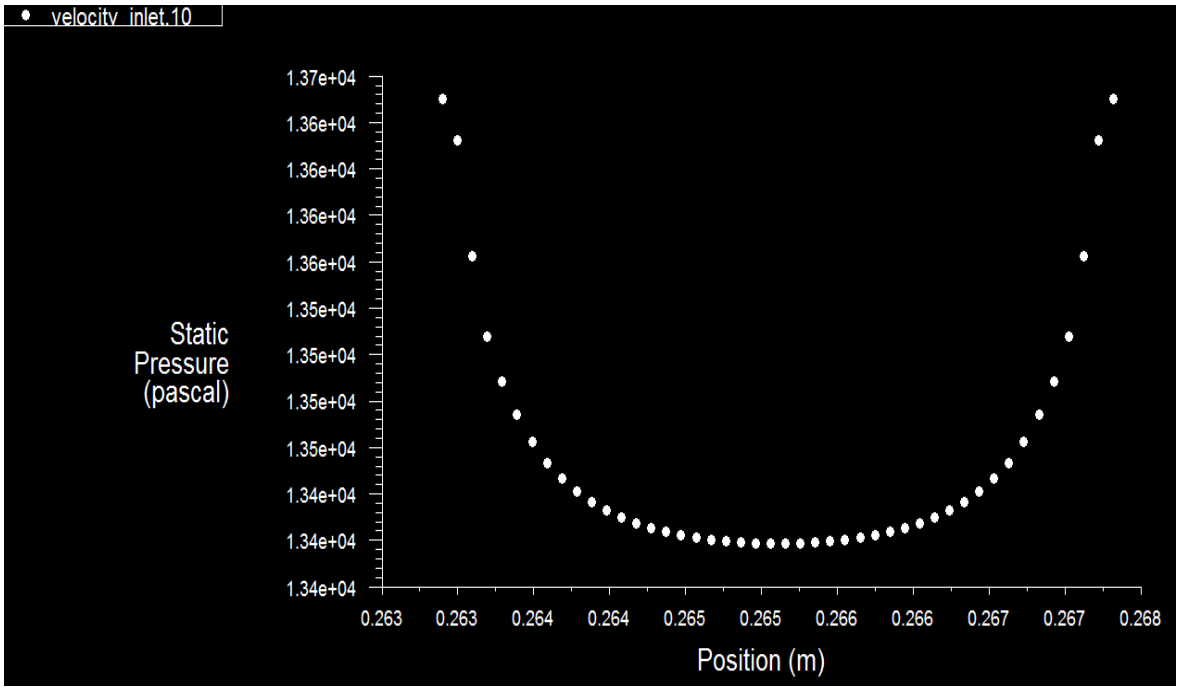

Fig 4.8: xy plot of Static Pressure at inlet in case 2.

Fig 4.8 shows the variation of the pressure at the inlet in xy dimension in case2 of the study.

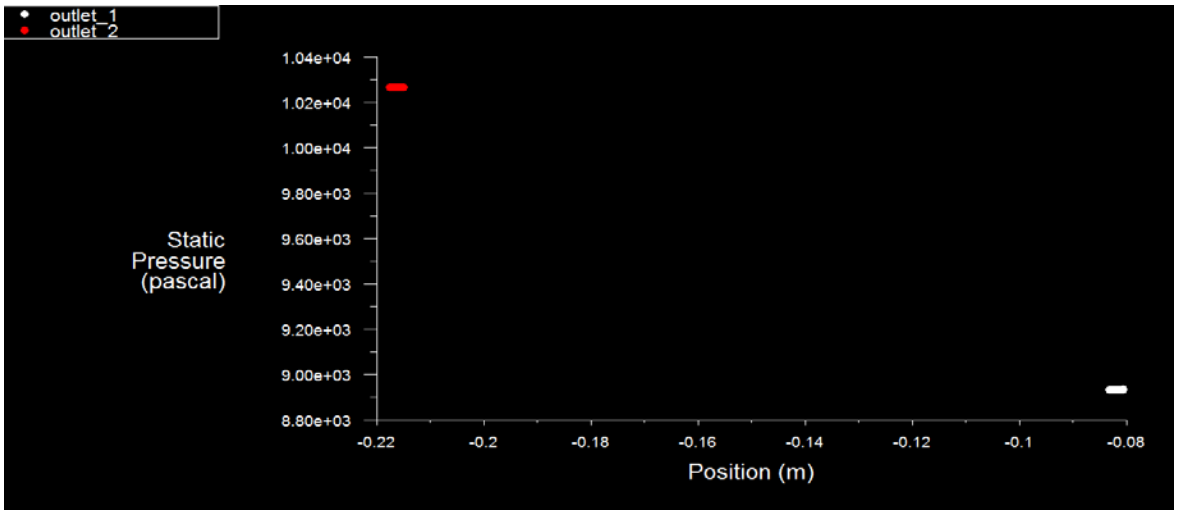

Fig 4.9: xy plot of Static Pressure at outlets in case 2.

Fig 4.9 shows the variation of static pressure at the outlet1 and outlet2 in the brachial artery in xy dimension curve. It is clear from the analysis of the Table 4.2 and from the Fig 4.7 and 4.9 that the pressure drop between the inlet and outlet is 3920 Pascal.

4.3: Case 3

Multiphasic flow in the brachial artery was performed and the outcome is represented in table 4.3

Table 4.3: Mass Weighted Average Surface integrals of flow in case3

Case 3	
Pressure inlet	4020 Pascal
Pressure Interior	2511.506 Pascal
Pressure outlet	240.04 Pascal
Velocity interior	0.6767 m/s
Velocity outlet	0.653 m/s
wall shear stress inlet	2.77 Pascal
wall shear stress interior	0.209 Pascal
wall shear stress outlet	0.427 Pascal
Pressure Change	0 mm/Hg

It is clear from the above table that multiphasic is not conclusive in case of the immune complex and there is no change in pressure drop across the length because in this case immune complex and blood is considered as the two different phases. However, the blood is flowing as a single phase in the artery and not multiphasic because immune complexes are not partitioning themselves in a distinct phase in the continuous stream.

4.4: Case 4

After this the disease conditions of three autoimmune diseases (systemic lupus erythematosus, rheumatoid arthritis, and glomerulonephritis) were studied with the available parameters in single phasic flow. Below are contours of pressure drop and velocity distribution across the length in normal individuals of Systemic Lupus Erythematosus.

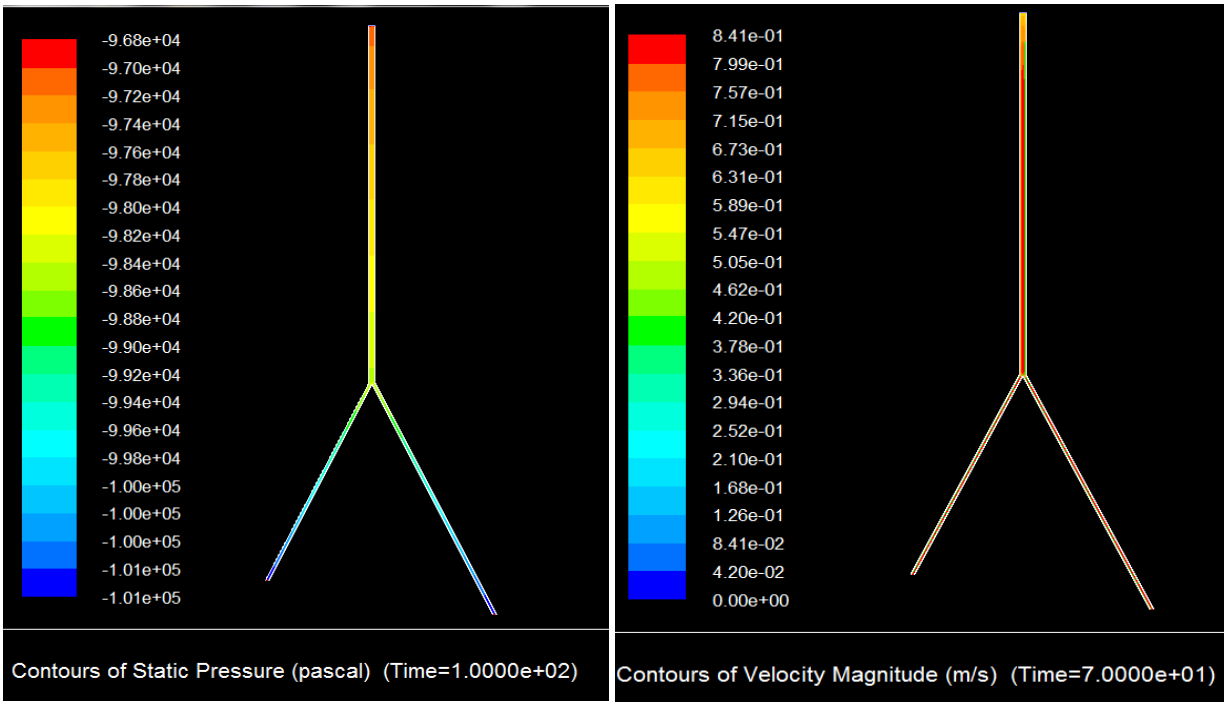

(a) (b)

Fig 4.10: Contours (a), (b) of Static Pressure and Velocity change respectively in the normal individuals of Systemic Lupus Erythematosus.

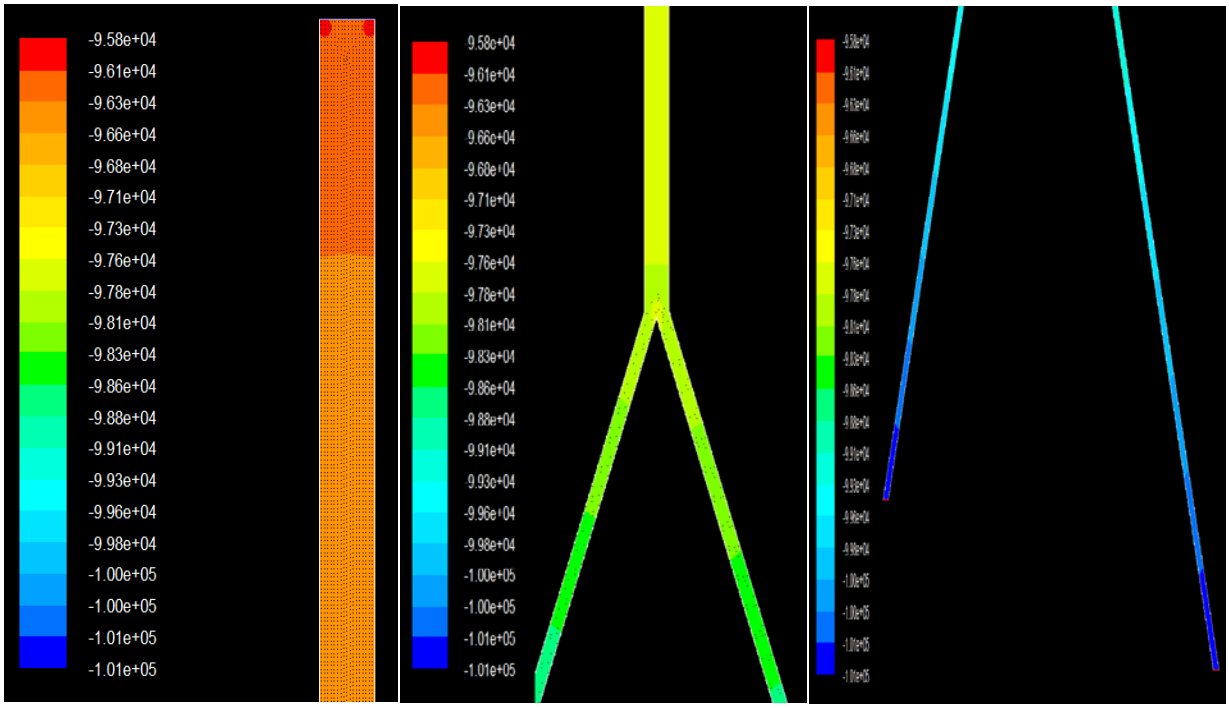

(a) (b) (c)

Fig 4.11: Pressure contours (a),(b),(c) at inlet ,bifurcation and outlet respectively for the SLE condition.

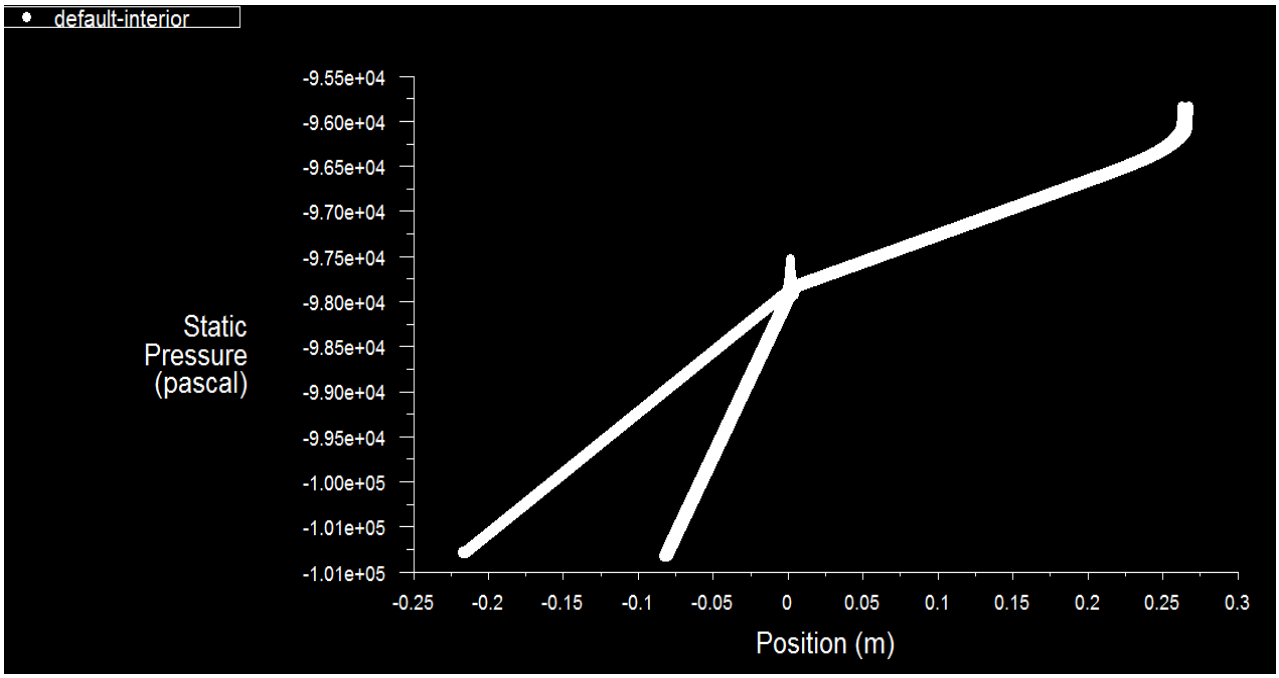

Fig 4.12: xy plot of Static pressure in SLE condition.

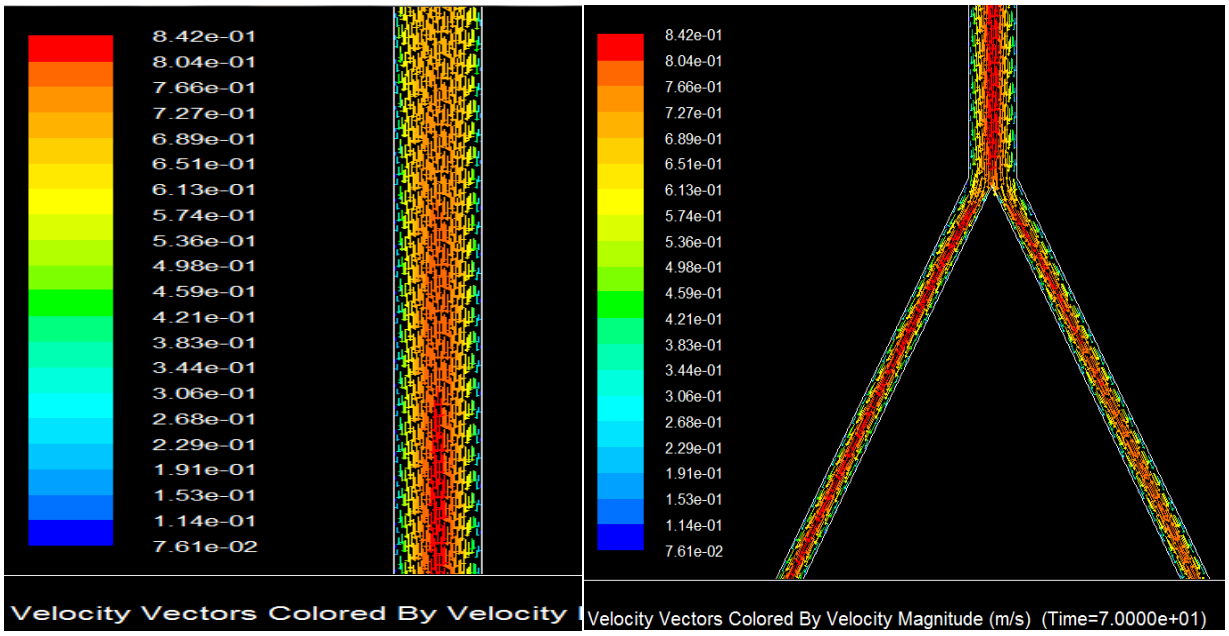

(a) (b)

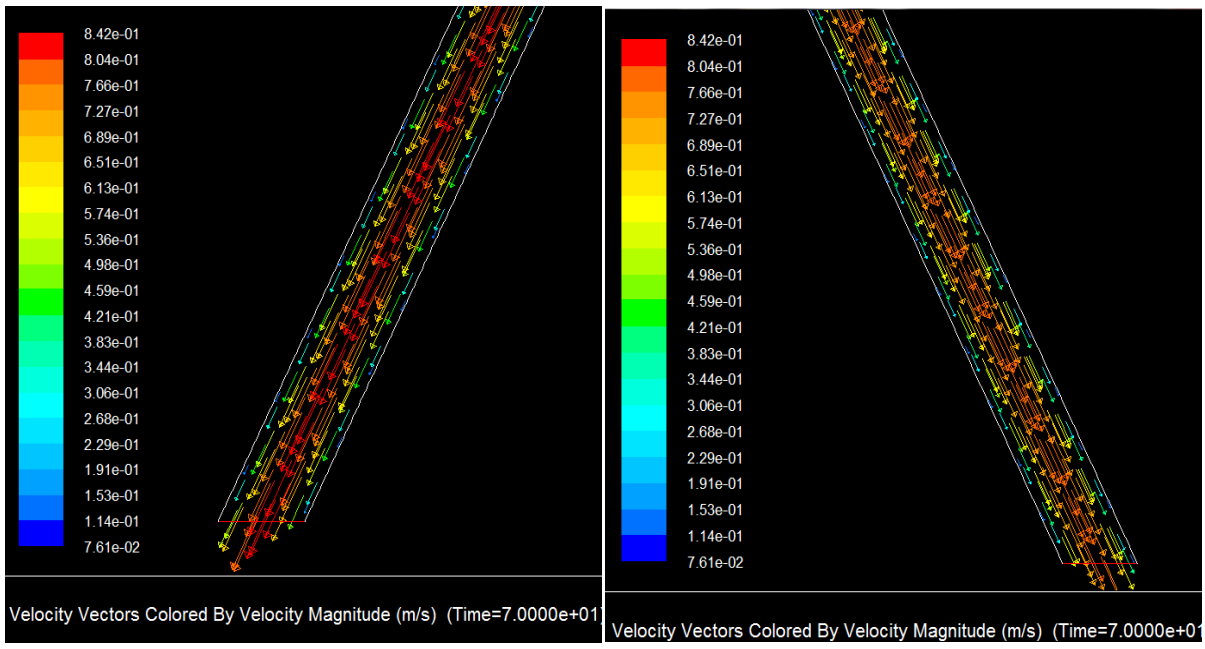

(c) (d)

Fig 4.13: Vectors of Velocity magnitude (a, b, c, d) of SLE at inlet, bifurcation and outlet 1,2 respectively.

The table below shows the surface integrals mass weighted average of the pressure change and velocity change in the normal individuals and patients. The comparative pressure drop between normal and patients is 9.6 mm/Hg. And there is also small change in the velocity of flow. The wall shear rate at inlet is also comparably high in the patients, implying that the heart has to pump more blood and will eventually cause elevation in blood pressure.

Table 4.3: Mass Weighted Average Surface integrals of the case under study i.e. Systemic Lupus Erythematosus

Systemic lupus Erythematosus		
	Normal Individuals	Patients
Static Pressure Inlet (Pascal)	-97038.67	-95741.12
Static Pressure Interior (Pascal)	-98564.27	-97966.77
Net Pressure Outlet (Pascal)	-100822.93	-100805.5
Pressure loss (Pascal)	3784.26	5064.38
Net Outlet Velocity (m/s)	0.6530101	0.65918
Inlet Velocity (m/s)	0.61111	0.61111
Wall shear Stress inlet (Pascal)	2.775	3.862
Pressure Change (mm/Hg)	9.60201964	

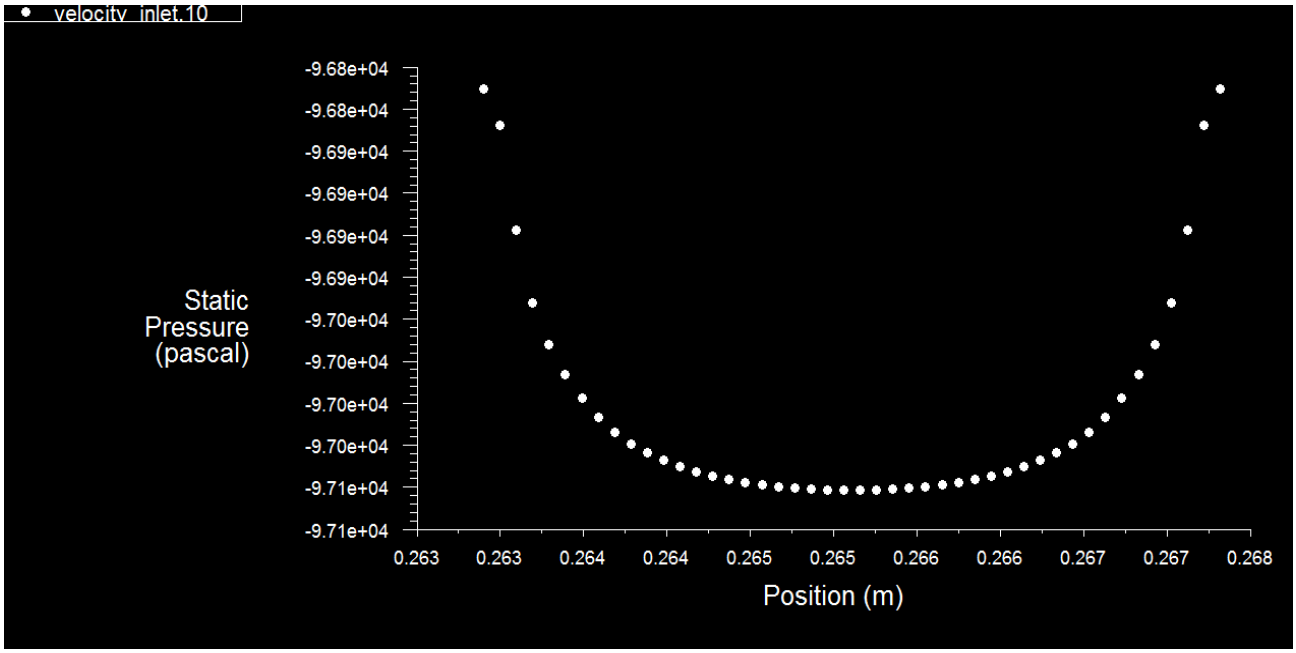

(a)

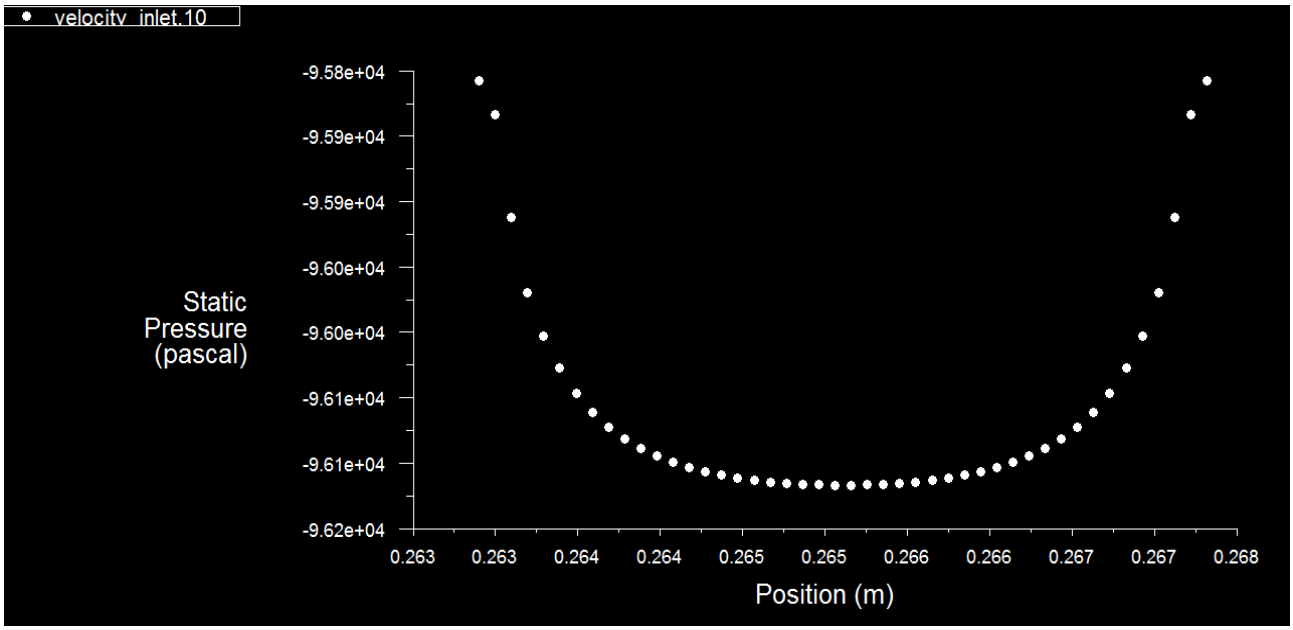

(b)

Fig 4.14: xy plot of Static Pressure (a), (b) at inlet in normal and SLE patient.

Above figure is showing the variation of static pressure at the inlet in xy dimension in the case of normal condition i.e. (a) and disease condition of Systemic Lupus i.e. (b).

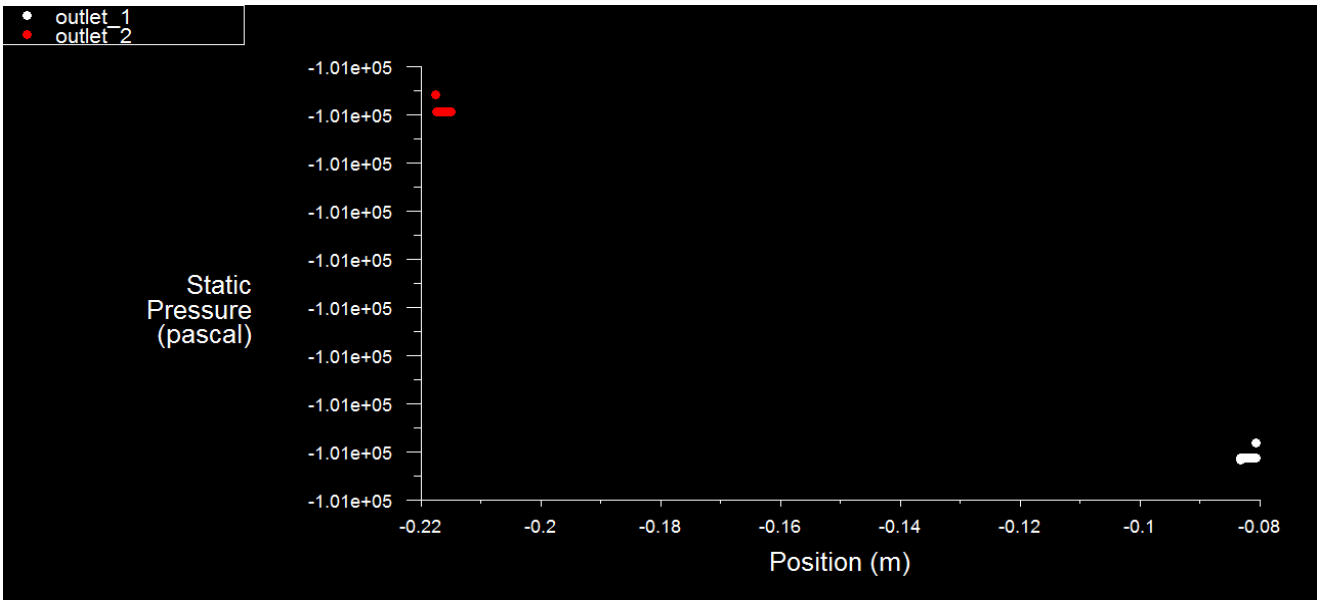

(a)

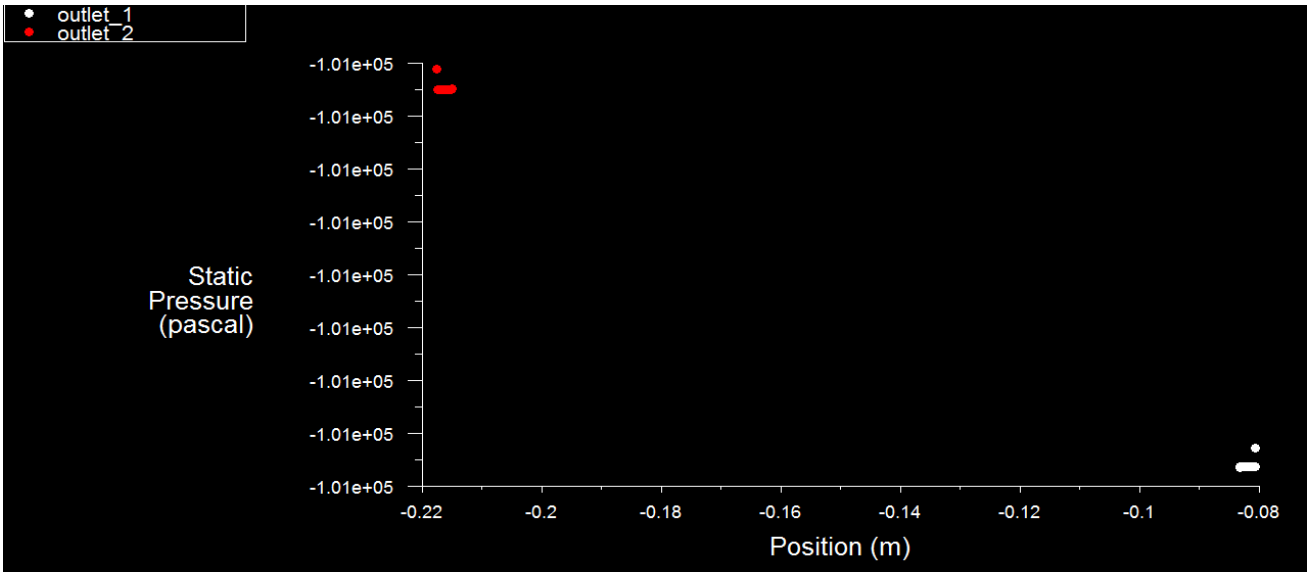

(b)

Fig 4.16: xy plot of Static Pressure (a), (b) at outlets of normal and SLE patients.

Fig 4.16 (a), (b) showing the comparative pressure drop at the outlet in both the case of normal condition and disease condition respectively in the Systemic Lupus Erythematosus.

From fig 4.10 and fig 4.11 is clear that the pressure drop is more in case of the disease condition. It is clear from the Table 4.3 that the comparative pressure drop between normal and affected individuals is around 1280 Pascal which upon conversion accounts to 9.6 mm/Hg, means this much is the extra amount of work heart has to do in order to compensate which automatically results in increase in blood pressure across the artery which is significant for the coronary complications according to the Wilson *et.al*. 1998. The change in velocity is around 0.05 m/s which is comparable with the pressure change and the wall shear stress change is negligible as the geometry was considered as rigid.

4.5: Case 5

The other case is of Glomerulonephritis; in this the contours are showing change in pressure across the length of Brachial Artery. The pressure drop across the length is more in case of Glomerulonephritis as compared with other diseases in study, as the flow and deposition of immune complexes is more in this case. Below are the contours of inlet, middle and outlet of the Brachial Artery in case of Glomerulonephritis.

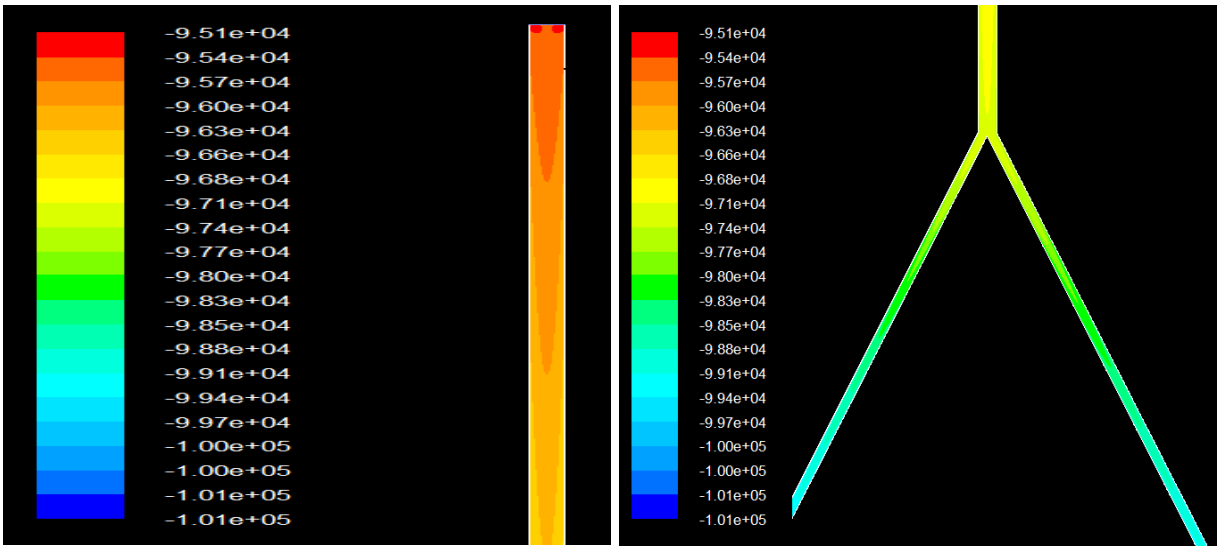

(a) (b)

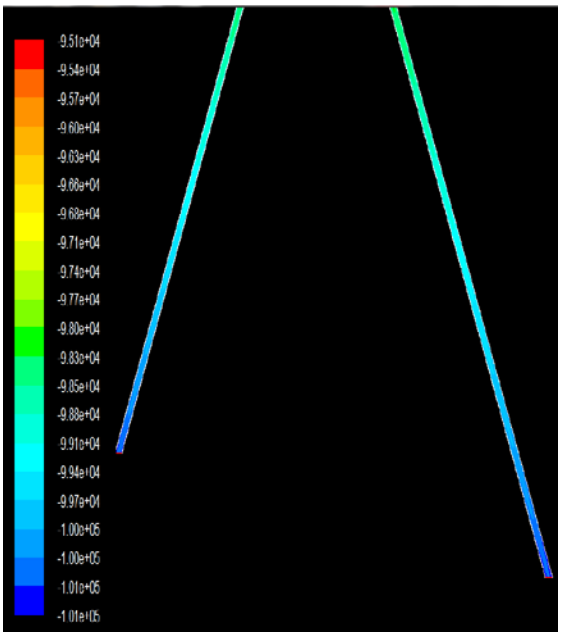

(c)

Fig 4.17: Static Pressure contours (a),(b),(c) at inlet ,bifurcation and outlet respectively for Glomerulonephritis patient.

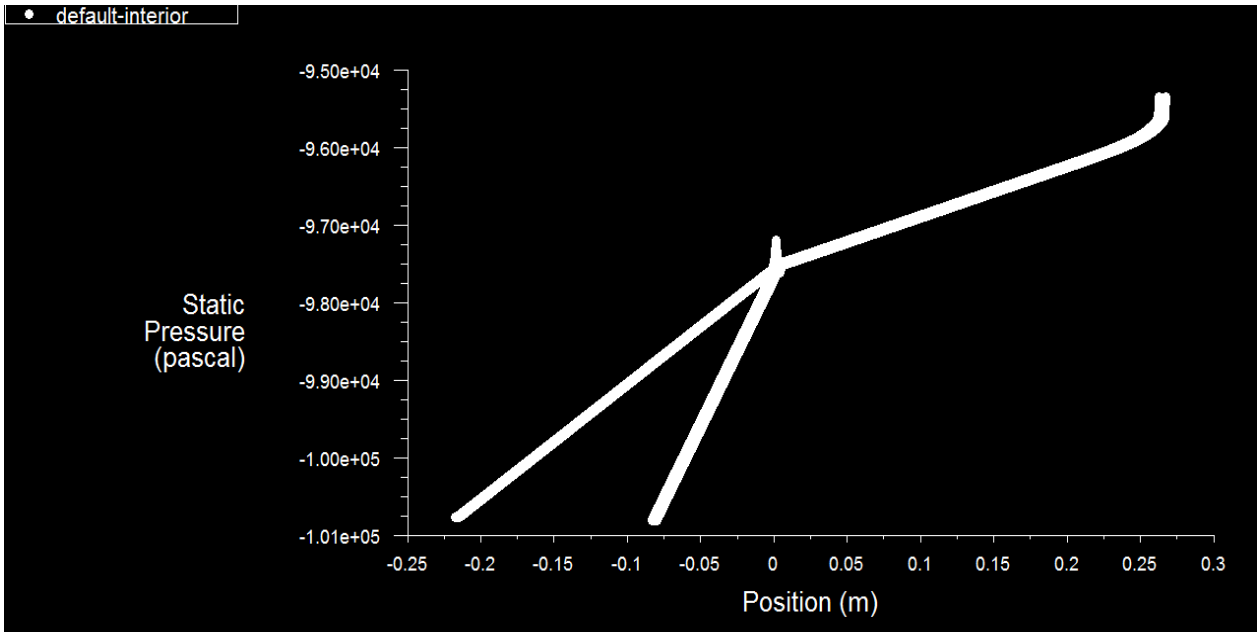

Fig 4.18: xy plot of Static Pressure in Glomerulonephritis condition.

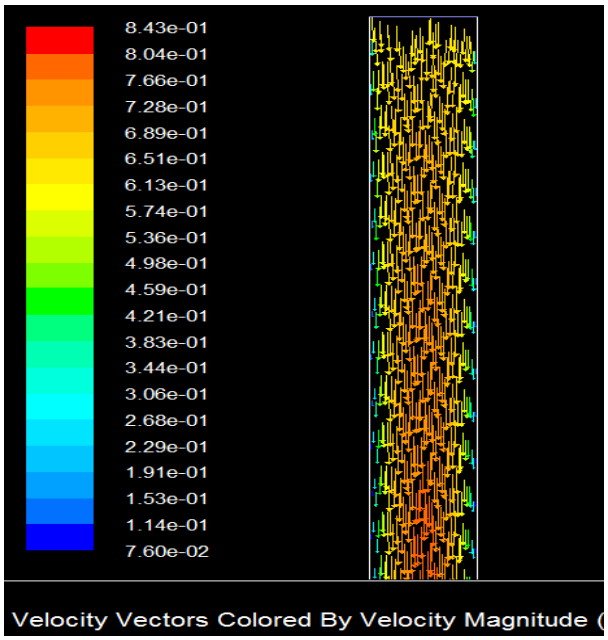

(a)

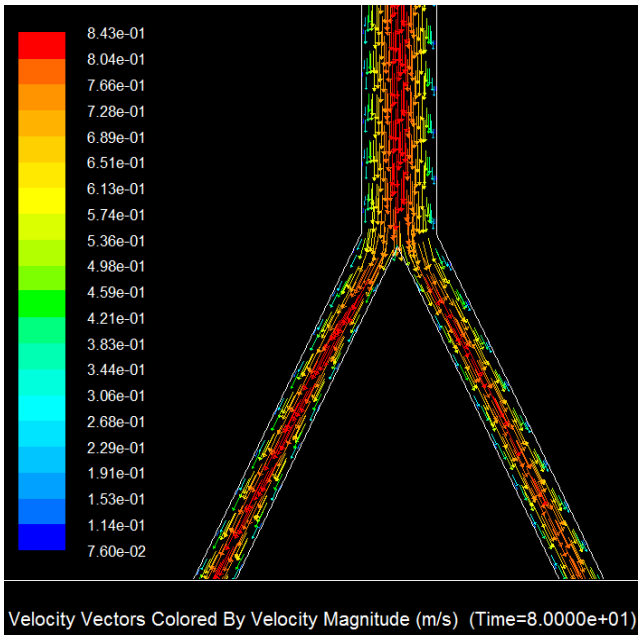

(b)

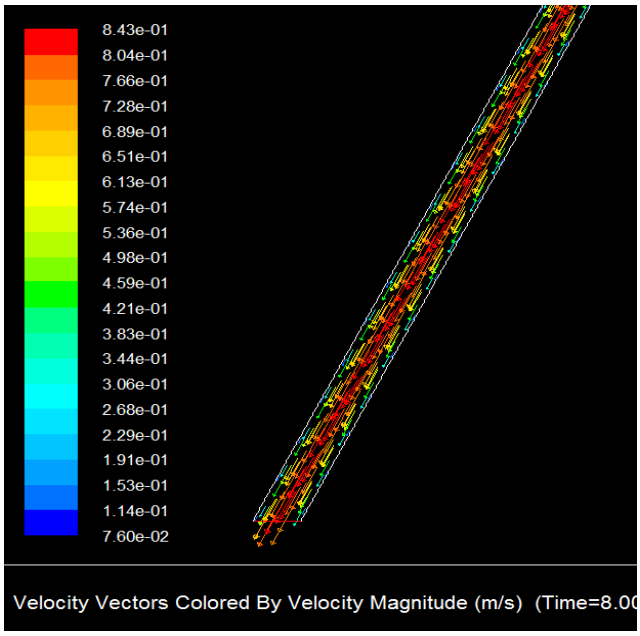

(c)

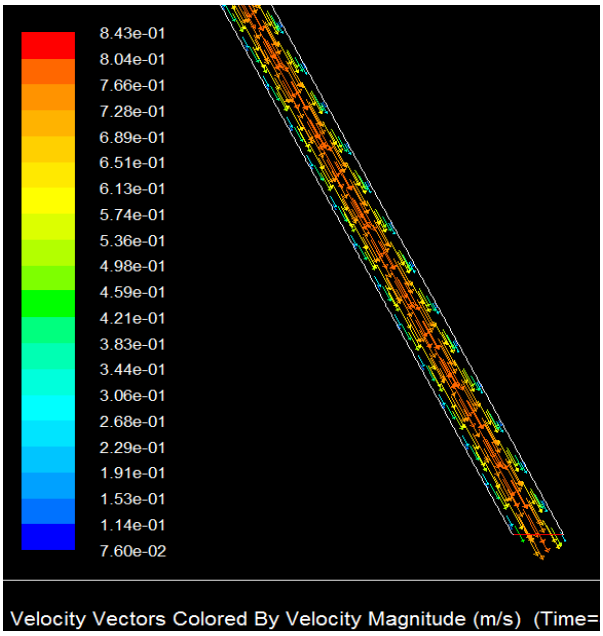

(d)

Fig 4.19: Vectors of Velocity magnitude (a, b, c, d) of patient at inlet, bifurcation, outlet1, 2 respectively.

The table below shows the surface integrals mass weighted average of the pressure change and velocity change in the normal individuals and patients. The comparative pressure drop between normal and patients 1, 2, 3 are 10.24, 10.09, 9.81 mm/Hg respectively and this averages to around 10mm/Hg. And there is also small change in the velocity of flow. The wall shear rate at inlet is also comparably high in the patients, means it is showing the increase in the pumping of the heart.

Table 4.4: Mass Weighted Average surface integrals of the case under study i.e. Glomerulonephritis

Glomerulonephritis				
	Normal Individuals	Patient1	Patient2	Patient3
Static Pressure Inlet (Pascal)	-97003.19	-95640.21	-95670.76	-95709.02
Static Pressure Interior (Pascal)	-98562.96	-97671.14	-97698.27	-97700.03
Net Pressure Outlet (Pascal)	-100822.79	-100793.24	-100804.68	-100805.5
Pressure loss (Pascal)	3819.61	5153.429	5134.1	5096.48
Net Outlet Velocity (m/s)	0.6656	0.661	0.659	0.659
Inlet Velocity (m/s)	0.6111	0.6111	0.6111	0.6111
Wall shear Stress inlet (Pascal)	2.7758	4.402	3.86	3.86
Pressure Change (mm/Hg)	10.24334488		10.09836546	9.816192253

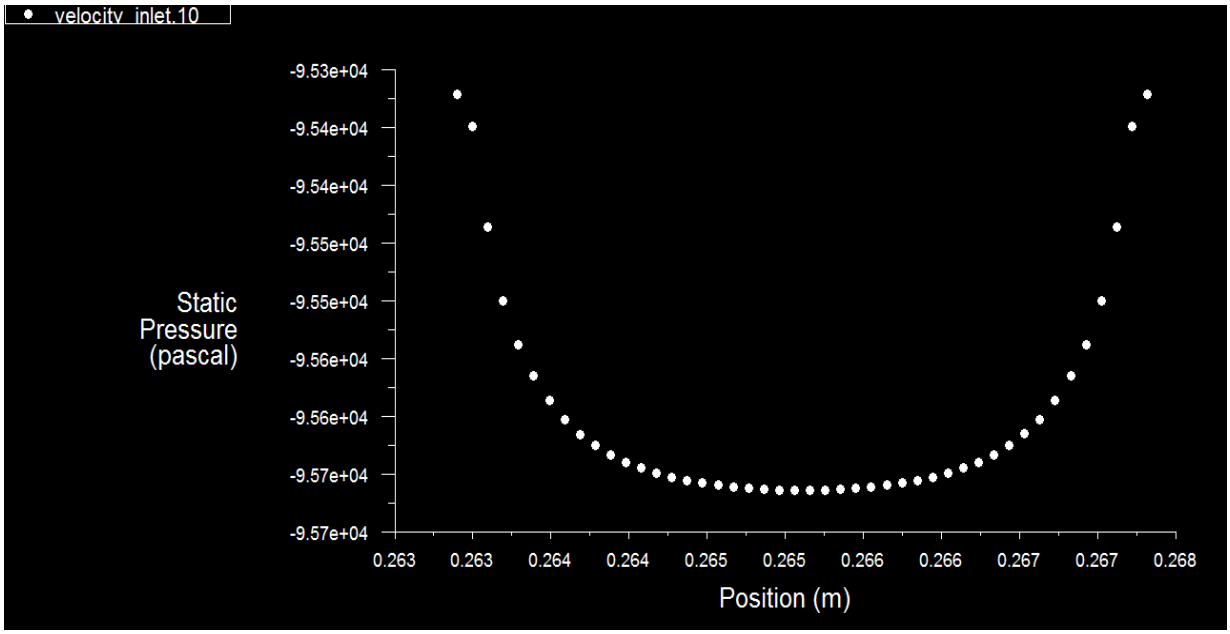

Fig 4.20: xy plot of Static Pressure at inlet in case 5.

Above figure is showing the pressure variation at the inlet in the Glomerulonephritis condition in xy dimension.

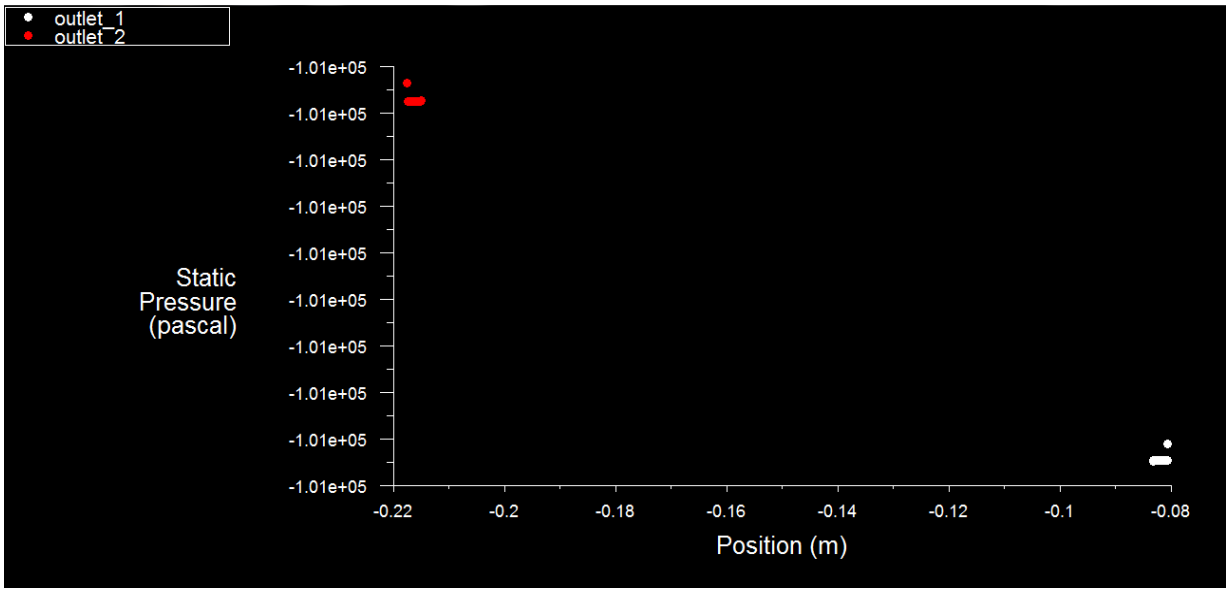

Fig 4.21: xy plot of Static Pressure at outlets in case 5.

In case of Glomerulonephritis condition there are large immune complexes that have a tendency of deposition in the organs or inside the artery so to simulate the same clinical condition of deposition. The concept of the discrete phase flow of immune complex in the blood stream with the trapping of the immune complex at the flow was used to simulate the clinical condition of deposition of immune complex in the glomeruli of kidney results in the disease glomerulonephritis. It is clear from the Table 4.4 the comparative pressure drop between normal and patients 1, 2, 3, is around 1367, 1348, 1310 Pascal respectively which upon conversion accounts to 10.25, 10.11, 10.06 mm/Hg respectively, and this averages to around 10 mm/Hg and it means that this much is the extra amount of work heart has to do in order to compensate which automatically results in increase in blood pressure across the artery which may lead coronary complications according to Wilson *et.al*. 1998. The change in velocity is around 0.05 m/s which is comparable with the pressure change and the wall shear stress change is negligible as the geometry was considered as rigid in this case also.

4.6: Case 6

In case of Rheumatoid Arthritis the contours are showing the change in pressure across the length of the artery. The pressure drop in this case is similar to the condition systemic lupus erythematosus. Below are the contours of the pressure drop across the length i.e. inlet, bifurcation and outlets.

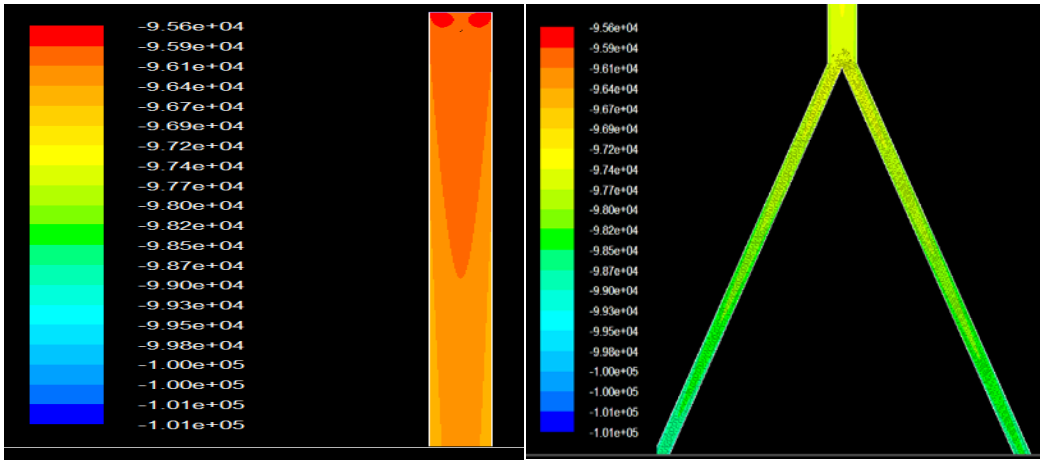

(a) (b)

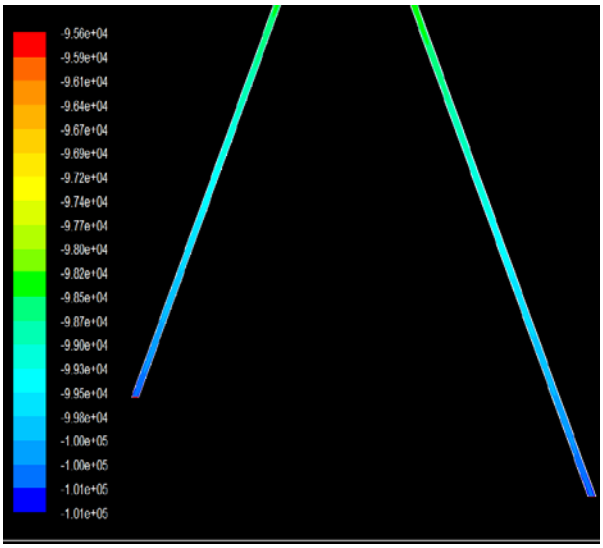

(c)

Fig 4.22: Contours of Static Pressure (a),(b),(c) at inlet ,bifurcation and outlet respectively for Rheumatoid Arthritis patients.

In the above figure the static pressure contours are showing the variation in the pressure drop across the artery, it is clear from the contours that the pressure drop is occurring maximum at the bifurcation of the brachial artery.

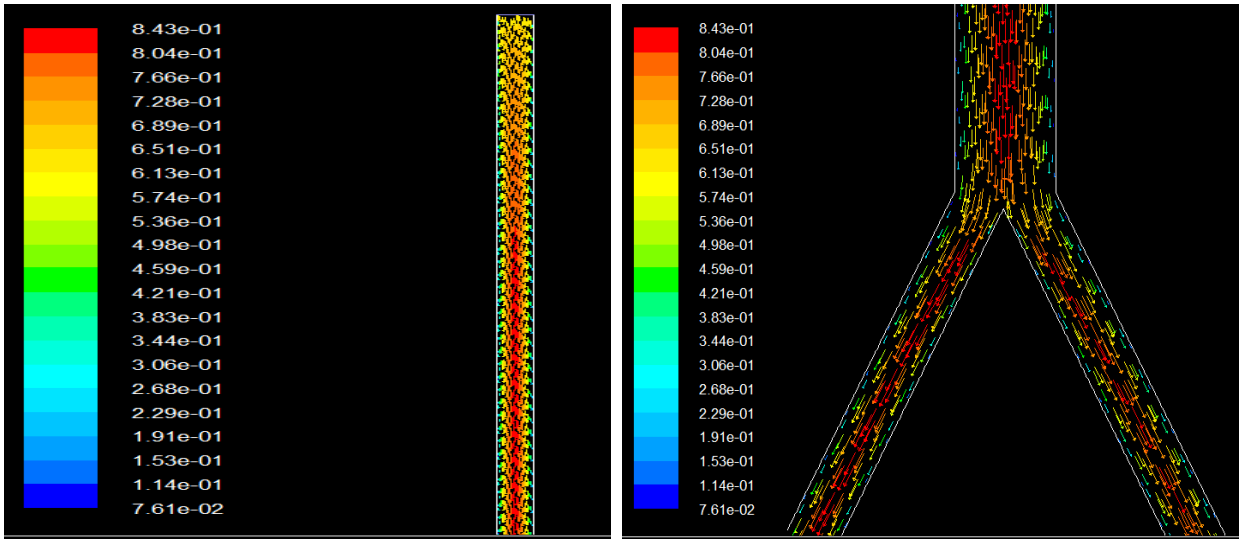

(a) (b)

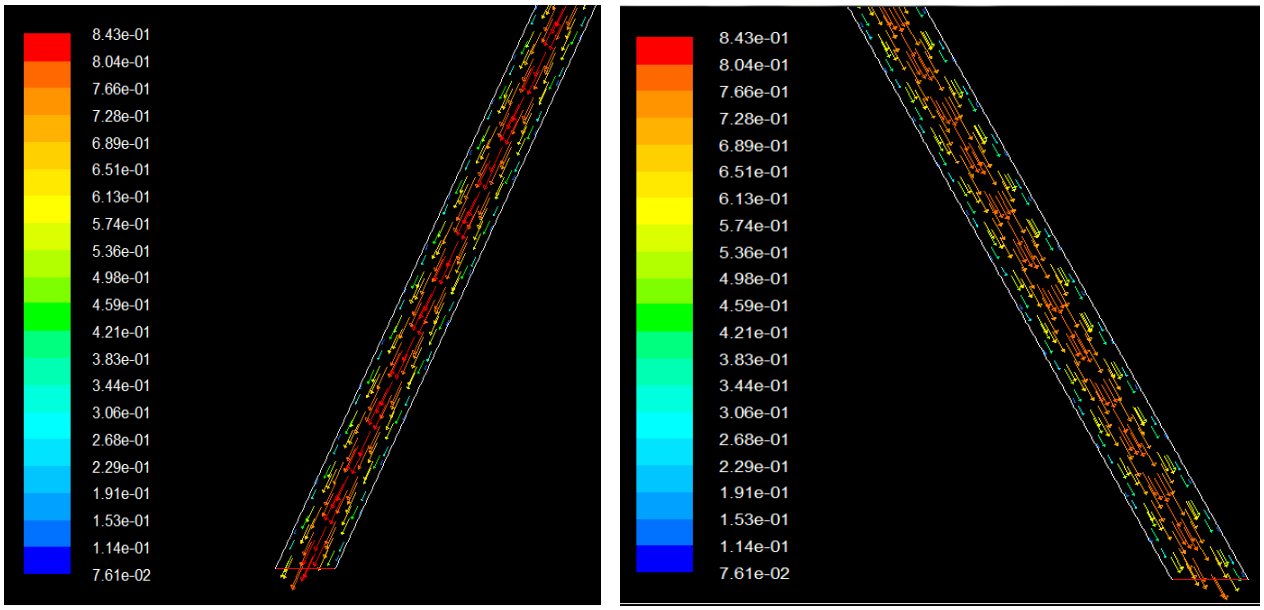

(c) (d)

Fig 4.23: Vectors of velocity magnitude (a, b, c, d) of Rheumatoid Arthritis patients at inlet, bifurcation, outlet1,2 respectively.

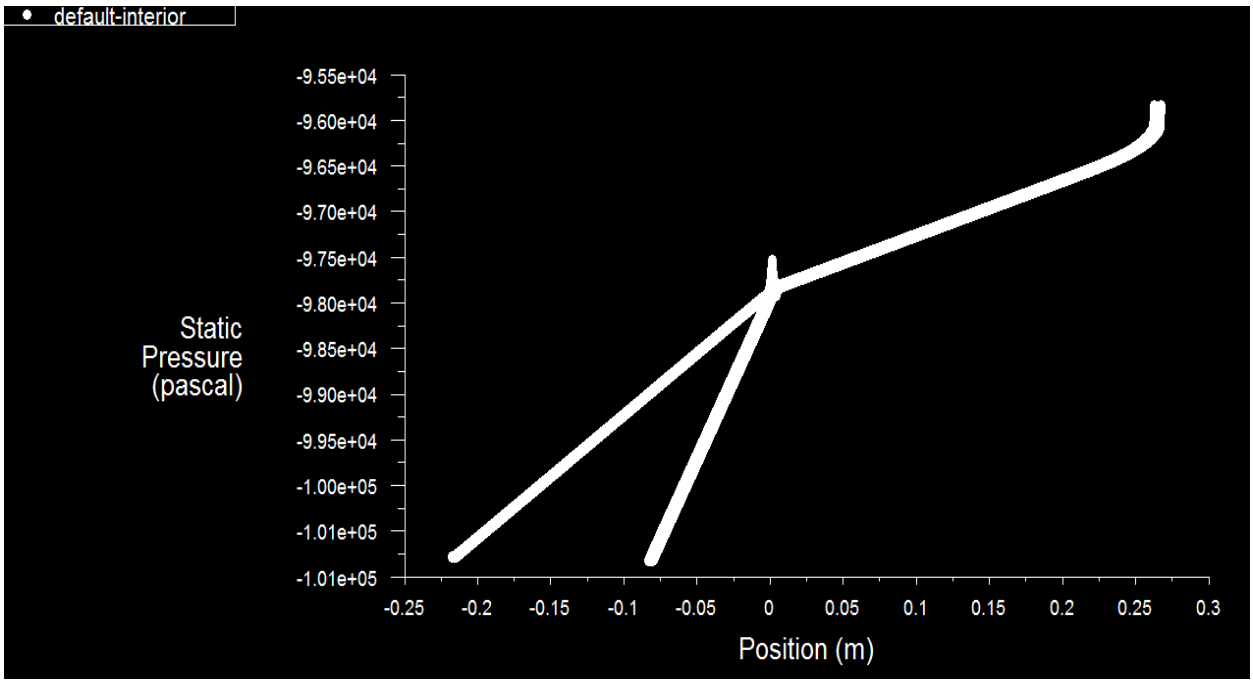

Fig 4.24: xy plot of static pressure in Rheumatoid arthritis patients with extra articular diseases.

The xy plot of the static pressure is showing the variation in pressure drop across the artery and it can be inferred from the plot that the values of static pressure are continuously decreasing from the values at the inlet.

The table below shows the surface integrals mass weighted average of the pressure change and velocity change in the normal individuals and patients. The comparative pressure drop between normal and patients with articular and extra articular diseases is 8.85 and 9.27 mm/Hg respectively and this averages to around 9mm/Hg. And there is also small change in the velocity of flow. The wall shear rate at inlet is also comparably high in the patients, means it is showing the increase in the pumping of the heart.

Table 4.5: Mass Weighted Average surface integrals of Rheumatoid Arthritis

Rheumatoid Arthritis			
	Normal Individuals	Patients with Articular	Patients with Extra Articular
Static Pressure Inlet (Pascal)	-96825.02	-95860.2	-95811.94
Static Pressure Interior (Pascal)	-98309.284	-98261.72	-97966.665
Net Pressure Outlet (Pascal)	-100582.91	-100799.6	-100805.52
Pressure loss (Pascal)	3757.89	4938.4	4994.753
Net Outlet Velocity (m/s)	0.653	0.6565	0.659
Inlet Velocity (m/s)	0.61111	0.6111	0.6111
Wall shear Stress inlet (Pascal)	2.7757	3.32	3.862
Pressure Change (mm/Hg)	8.85455317		9.277235431

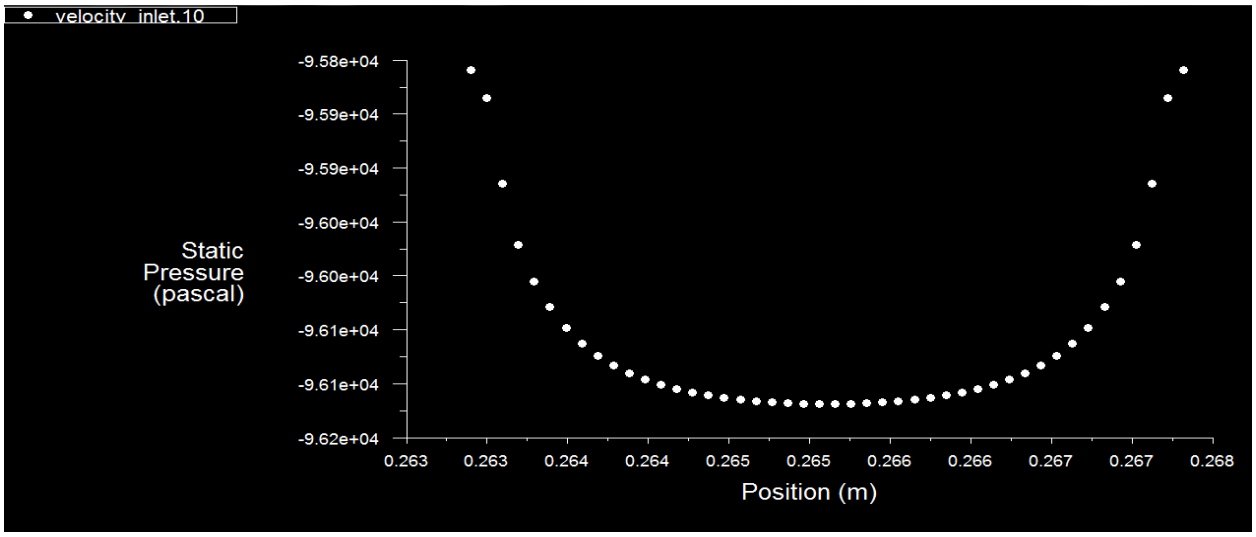

Fig 4.25: xy plot of Static Pressure at inlet of case 6.

The above figure is showing the static pressure variation curve at the inlet in condition of Rheumatoid Arthritis in the xy dimension.

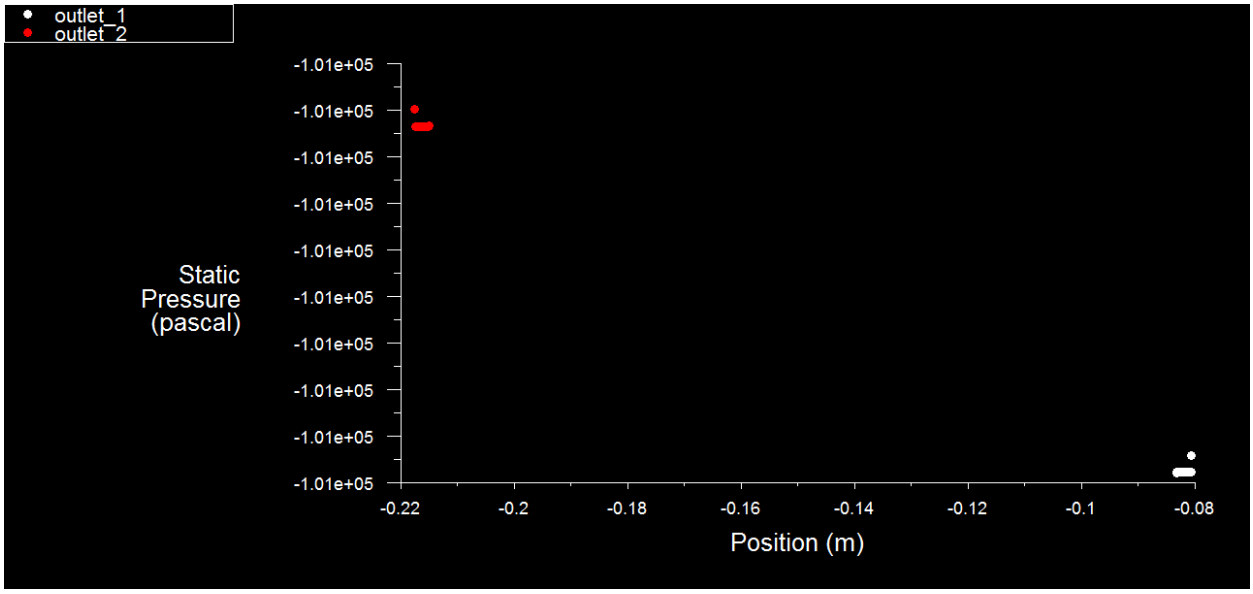

Fig 4.26: xy plot of Static Pressure at outlet in case 6.

The above figure is showing the static pressure variation at the outlet with red dot being the outlet2 and white is outlet1 in xy dimension.

Now, it is clear from the Table 4.5 that in the case of Rheumatoid Arthritis the comparative pressure drop across the length between control subjects and individuals with articular and extra articular diseases is around 1181 and 1236 Pascal respectively which upon conversion accounts to around 9.3, 9 mm/Hg respectively, and these values averages to around 9.1mm/Hg and may be alarming for coronary complication according to Wilson et.al. 1998. The change in velocity is around 0.05 m/s which is comparable with the pressure change and the wall shear stress change is around negligible as the geometry was considered as rigid in this case also.

In the case of Rheumatoid Arthritis and Systemic Lupus there is very less deposition of immune complex and the amount of immune complex is also very less as compared to the Glomerulonephritis condition so the escaping of discrete phase is simulated in Rheumatoid Arthritis and Systemic Lupus. The change in pressure drop across the artery in case of Glomerulonephritis is more as compared to the other two diseases in study because of the high amount of immune complex in glomeruli. The average change in pressure drop is near about to 10 mm/Hg in all the diseases and shows that around 80% risk of coronary complications may be predicted in these disease. Prognosis of coronary complications and disease progress in genetics may be assessed using the CFD analysis.

Chapter 5 Discussion

CFD analysis is an effective method to simulate fluid flow through arteries with the construction of suitable geometrical model. It has wide ranging applications in the area of fluid flow and thermal simulations. Huge number of research work has been carried out in bio-medical field, specifically arterial blood flow, so far, using these tools and techniques. CFD has been used to find the pressure drop and velocity change across the geometry specified. A diverse number and varieties of arterial model have been studied in evaluating the stenosed condition of arteries.

After an extensive literature review it has been found that no serious computational or simulation work has been carried out for the flow simulation in brachial artery. Therefore, the present study is aimed to prognose the pressure change in the brachial artery resulting due to higher concentration of immune complexes with the help of Computational Fluid Dynamics.

The blood flow in the Brachial Artery is simulated and complications resulting from the addition of immune complexes in the blood have been assessed.The main objective has been to calculate the change in pressure drop across the length of artery and the comparative pressure drop between healthy individuals and patients that will give the extra amount of work done by heart i.e. the increased blood pressure that the patient has to bear. In autoimmune disease there is a load of immune complexes involving large numbers of autoantibodies that are flowing in the blood which leads to the change in blood pressure, however the diagnosis is carried out only upon onset of clinical condition which is very late in disease progression.

In the present study the blood flow in normal anddisease condition was simulated and the change in pressure drop was calculated. For this, first of all in case1 the flow parameters were standardized and the velocity rates in the artery using the fixed parameters of pressure were analyzed. In case1 the inlet and outlet pressures were fixed and the consequent change in velocity across the artery and the change in wall shear stress were calculated. So with this the velocity profile was determined that how velocity changes in the artery with that much pressure difference. Now in case2 the average inlet velocity from the literature and outlet pressure is used

to calculate the inlet pressure that develops due to the velocity and outlet pressure. So change in pressure across the artery with the inlet velocity is calculated across the artery. After standardizing the change in pressure and velocity values across the length it was thought to flow the blood in multiphase condition considering the autoimmune complexes as the different phase.

As the autoimmune complexes in the rheumatoid arthritis and glomerulonephritis have tendency to get deposited in the synovial joints and in kidney respectively, so trial to simulate it in case3 in multiphase condition was failed to produce any results because the insertion of the parameters for the different phases have not been possible in the steady state and for this the user defined function is to be inserted for that.

So dropping the idea for simulation in multiphasic flow, now the discrete phase flow of the immune complex in the single phase of the blood flow was performed. On this basis case4 study was performed with the normal condition and the disease and the inlet velocity as posited by K.A. Illig*et.al.* 2005 and outlet flow rates were used which led to calculate the change in pressure drop across the artery.

In this the application continuity equation follows according to which the amount of blood which has entered the artery is equal to the sum of the blood getting out from the two outlets. The comparative pressure drop in the normal condition and the disease condition is upto the significant level of coronary complications. Same was in the case 5 and case 6 of Glomerulonephritis and Rheumatoid Arthritis respectively. Inlet velocity and outlet flow rates were used to calculate the pressure drop and velocity change across the artery. In case5 and case6 immune complexes were too much heavy that was having the tendency to get deposited inside the layers of the vessel or in the joints in case of glomerulonephritis. So discrete phase flow with the trapping of immune complex at each level of the flow was performed to calculate the change across the artery. As desired, the change in pressure drop calculated was better than expected. Hence, based on the case studies represented in the present project the comparative pressure drop calculated in the disease level is around 10 mm/Hg which is a significant indicative of risk for coronary complications as elaborated by Wilson *et.al*. 1998.

Some more research has to be performed with other autoimmune diseases so that this simple non invasive therapy using the blood drop to check the immune level and change in blood pressure can be incorporated to prognoses the autoimmune disease coronary complications at the level of onset of disease.Autoimmune therapeutic evaluation is another aspect of CFD analysis; autoimmune diseases are detected at very late stage. In addition at this time several other factors also start playing role. Moreover, the drugs available, suppresses the entire immune system of body, so more specific drugs are required for better treatment. CFD analysis could be used for evaluation of new techniques because it provides ideal condition.

Chapter 6 Conclusion

In the present study the blood flow inside brachial artery is simulated using computational fluid dynamics and the change in pressure is determined. In autoimmune diseases high amounts of autoantibodies and immune complexes formed lead to high blood viscosity. Computational fluid dynamics provides a suitable platform to study the effect of circulating immune complexes on blood pressure by comparing normal and disease condition. The comparative pressure drop in each case was detected and the difference in the pressure was calculated. The comparative pressure drop between the normal and disease condition shows the extra amount of work done by heart to maintain the same blood flow parameters with a comparatively high blood viscosity. In each of the autoimmune cases studied, a significant rise in blood pressure was detected (9-10.25 mm/Hg), which according to W. F. Wilson *et.al.*1998 implies possible onset of coronary complications. On the basis of pressure variation and concurrent detection of immune complex concentration in a single drop of peripheral blood, one can devise a prognostic method for accurate prediction of onset of coronary complications.

In the future some improvements to this model can be made as given below

- The model can be designed in 3D and assumptions such as blood being non- Newtonian and the blood vessel walls being rigid can be eliminated.
- Furthermore, the user defined functions can be used to create the pulsatile flow so that values can be more precise up to higher significant levels.
- Several different turbulent solvers (k-omega, k- epsilon, etc.) can be used and the results can be compared side-by-side.

References

Anayiotos AS, Jones SA, Giddens DP, Glagov S, Zarins CK(1994). Shear stress in a compliant model of the human carotid bifurcation. **Journal of Biomechanical Engineering**. 116:98-106.

Avolio, A. (1980). Multi-branched model of the human arterial system. **Med & Biol Eng & comput,** Vol. 18, 709-718.

Bardana, E.J., JR, Harbeck, R.J., Hoffman, A.A., Pirofsky, B. & Carr, I. (1973) The prognostic and therapeutic implications of DNA:anti-DNA immune complexes in systemic lupus erythematosus (SLE). **Am. J. Med.** 59, 515.

Balasubramanian, K (1979). An experimental investigation of steady flow at an arterial bifurcation. Georgia Institute of Techology Thesis.

Berger, S. & Jou, L. (2000). Flows in Stenotic vessels. **Annu Rev fluid Mech** , Vol. 32, 347-382.

B.F. Buxton, a.T. Chan, a.S. Dixit, N. Eizenberg, R.D. Marshall, and J.S. Raman(1998). Ulnar artery as a coronary bypass graft, **The Annals of thoracic surgery**, vol. 65, pp. 1020-4.

Carneiro, F.; Silva, A.; Teixeira, S.; Teixeira, J.; Lobarinhas, P. & Ribeiro, V. (2008a). The Influence of Renal Branches on the Iliac Arteries Blood Flow, Proceedings of the A5ME 3rd rontiers in Biomedical Devices, 0791838234, Irvine, California, June 2008.

Carneiro, F.; Ribeiro, V.; Teixeira, S. & Teixeira, J. (2008b) Numerical study of blood fluid analogous in the abdominal aorta bifurcation, Proceedings of 7th International conference on comparing Design in Nature with 5cience and Engineering, 97818456412072426, Algarve, June 2008, WIT Press, Southampton.

Caro CG, Pedley TT, Schroter RC, Seed WA (1978). The Mechanics of the Circulation.

Oxford University Press, New York.

Castro MA, Putman CM, Cebral JR.(2006). Patient-specific computational modeling of cerebral aneurysms with multiple avenues of flow from 3D rotational angiography images. **Acad Radiol;13(7)**:811—21.

Cebral, J.; Yim, P.; Lohner, R.; Soto, O. & Choyoke, P. (2002). Blood flow modeling in carotid arteries with computational fluid dynamics and MR imaging. **Acad Radiol** Vol. 9, 1286-1299.

Cochrane C G, Hawkins D.(1968). Studies on circulating immune complexes-III. Factors governing the ability of circulating complexes to localize in blood vessels. **J Exp Med; 127**: 137-54.

Cameron, J.S., Lessof, M.H., Ogg, C.S., Williams, B.D. & Williams, D.G. (1976) Disease activity in the nephritis of systemic lupus erythematosus in relation to serum complement concentrations. DNA-binding capacity and precipitating anti- DNA antibody. **Clin. exp. Immunol.** 25,418.

Cano, P.O., Jerry, L.M., Sladowski, J.P. & Osterland, C.K. (1977) Circulating immune complexes in systemic lupus erythematosus. **Clin. exp. immunol.** 29, 197.

C.C. Botara, T. Vasileb, S. Sfrangeub, S. Clichicic, P.S. Agachia, R. Badeab, P. Mircead, M.V. Cristeaa. (2010).Validation of CFD simulation results in case of portal vein blood flow.

Cairncross RA, Schunk PR, Baer TA, Rao RR, Sackinger PA (2000) A finite element method for free surface flows of incompressible flu-ids in three dimensions, Part I: boundary fitted mesh motion., **Int. J. Numer. Meth. Fluids, 33**:375–403.

Chenghai Sun and Lance L. Munn (2005) .Particulate Nature of Blood Determines Macroscopic Rheology: A 2-D Lattice Boltzmann Analysis**. Biophysical Journal Volume 88 :**1635–1645.

Finnigan P, Hathaway A, Lorensen W (1990) Merging CAT and FEM, **Mech. Eng.,112:** 28–32.

Franklin E C, Holman H R, Muller-Eberhard H J, Kunkel H G.(1957) .An unusual protein component of high molecular weight in the serum of certain patients with rheumatoid arthritis. **J7 Exp Med; 105**: 425-38.

Gijsen FJH, van de Vosse FN, Janssen JD(1999). The influence of the non-Newtonian properties of blood on the flow in large arteries: steady flow in a carotid bifurcation model. Journal of Biomechanics. 32: 601-608.

He, S. & Jackson, J. (2000), A study of turbulence under conditions of transient flow in a pipe. **fluid Mech** , Vol. 408, 1-38.

Helmke, B. P., S. N. Bremne, B. W. Zweifach, R. Skalak, and G. W. Schmid-Schonbein. (1997). Mechanisms for increased blood flow resistance due to leukocytes. **Am. J. Physiol. 273**:H2884–H2890.

Hess, J.L.; A.M.O. Smith (1967). Calculation of Potential Flow About Arbitrary Bodies. **Progress in Aeronautics Sciences 8**: 1–138.

Jacobson DL, Gange SJ, Rose NR, Graham NM. (1997). Epidemiology and estimated population burden of selected autoimmune diseases in the United States**. Clin Immunol Immunopathol;84:**223-43.

Kagadis, G.; Skouras, E.; Bourantas, G.; Paraskeva, C.; Katsanos, K.; Karnabatidis, D. & Nikiforidis, G. (2008). Computational representation and hemodynamic characterization of in vivo acquired severe stenotic renal artery geometries using turbulence modeling. **Medical Engineering & Physics**, Vol. 30, 647-660.

K. S. K. Tung, R. J. Dehoratius & R. C. Williams,(1981). Study of circulating immune complex size in systemic lupus erythematosus. **Clin. exp. Immunol**. **43**, 615-625.

Korbet S M, Schwartz M M, Lewis E J.(1984) Immune complex deposition and coronary vasculitis in systemic lupus erythematosus. **Am J Med**; 77: 141-6.

Koffler, D., Schur,P.H. & Kunkel, H.G. (1967) Immunological studies concerning the nephritis of systemic lupus erythematosus. **J. exp. Med.** 126,607.

Krishnan, C. & Kaplan, M.H. (1967) Immunopathologic studies of systemic lupus erythematosus. II. Anti-nuclear reaction of y-globulin eluted from homogenates and isolated glomeruli of kidneys from patients with lupus nephritis. **J. clin. Invest**. 46, 569.

Ku, D. (1997). Blood flow in arteries**. Annu Rev fluid Mech**, Vol. 29, 399-434.

Lee, D. & Chen, J. (2002). Numerical simulation of steady flow fields in a model of abdominal aorta with its peripheral branches**. Journal of Biomechanics**, Vol. 35, 11151122.

Lee, D. & Chen, J. (2003). Pulsatile flow fields in a model of abdominal aorta with its peripheral branches. **Biomedical Engineering Applications, Basis & communications**, Vol. 33, 1305-1312.

Levinsky, R.J., Cameron, J.S. & Soothill, J.F. (1977) Serum immune complexes and disease activity in lupus nephritis. Lancet, **1**, 564.

L. Jou, C. M. Quick, W. L. Young, and M. T. Lawton,(2003) "Computational Approach to Quantifying Hemodynamic Forces in Giant Cerebral Aneurysms", **AJNR Am J Neuroradiol**, pp.1804–1810.

Li, Z. & Kleinstreuer, C. (2005), Blood flow and structure interactions in a stented abdominal aortic aneurysm model, **Medical Engineering & Physics**, Vol.27, 369-382.

Li, M.; Beech-Brandt, J.; John, L.; Hoskins, P. & Easson, W. (2007). Numerical analysis of pulsatile blood flow and vessel wall mechanisms in different degrees of stenoses**. Journal of Biomechanics**, Vol. 40, 3715-3724.

Milne-Thomson,L.M.(1973).TheoreticalAerodynamics.Dover Publications. ISBN 048661980X.

McDougal J S, McDuffie F C. (1985) Immune complexes in man: detection and clinical significance**. Adv Clin Chem; 24**: 1-60.

Morris L, Delassus P, Callanan A, Walsh M, Wallis F, Grace P, McGloughlin T. (2005) 3-D numerical simulation of blood flow through models of the human aorta. **J Biomech Eng;127(5)**:767—75.

Nanduri, J.; Pino-Romainville, F. & Celik, I. (2009). CFD mesh generation for biological flows: Geometry reconstruction using diagnostic images**.computers & fluids,** Vol. 38, 1026-1032.

O'Brien, V. & Ehrlich, L. (1977). Simulation of unsteady flow at renal branches. **journal of Biomechanics**, Vol. 10, 623-631.

Plebani M, Marincola(2006) FM. Research translation: a new frontier for clinical laboratories**. Clin Chem Lab Med**;44:1303–12.

Perktold K, Rappitsch G (1995) Computer simulation of local blood flow and vessel mechanics in a compliant carotid artery bifurcation model, **J. Biomech., 28 (7)**: 845–856.

Perktold K, Resch M, Peter RO (1991) Three dimensional numerical analysis of pulsatile flow and wall shear stress in carotid artery bifur-cation**. J. BioMech., 24**:409–20.

Perktold K, Rappitsch G, Löw M, Friedman MH, Kuban BD(1995). Computer simulation of pulsatile flow in an anatomically realistic human left coronary artery bifurcation model. **BED Advances in Bioengineering ASME**. 31:193-194.

Wilson Peter W. F., Ralph B. D'Agostino, Daniel Levy, Albert M. Belanger, Halit Silbershatz and William B. Kannel (1998; 97), Prediction of Coronary Heart Disease Using Risk Factor Categories**. Circulation**, 1837-1847.

Popel, A. S., and P. C. Johnson.(2005). Microcirculation and hemorheology. **Annual Review of Fluid Mechanics**. **37**:43–69.

R A Mageed, J R Kirwan, P W Thompson, D A McCarthy, E J Holborow (1991) Characterisation of the size and composition of circulating immune complexes in patients with rheumatoid arthritis. **Annals of the Rheumatic Diseases**; **50**: 231-236.

Rappitsch, G. & Perktold, K. (1996). Computer simulation of convective diffusion process in large arteries. **journal of Biomechanics**, Vol. 29, 207-215 .

Ransohoff DF(2004) Evaluating discovery-based research: when biologic reasoning cannot work. **Gastroenterology**;127:1028.

Reuderink PJ(1991). Analysis of the flow in a 3D distensible model of the carotid artery bifurcation. Eindhoven Technical University Thesis.

S. Echavarría , L. Giraldo, C.A. Pérez, R.A. Valencia and J. Bustamante.(2011). CFD Analysis of Blood Flow in Arteries with Stenosis**. Agosto.** 10-12.

S. M. Abdul Khader1_, B. Satish Shenoy1, Raghuvir Pai1, S. Ganesh Kamath2, Nabeel Md Sharif3, V. R. K. Rao3(2011). World Journal of Modelling and Simulation Vol. 7 No. 2, pp. 113-122.

Shahcheraghi N, Dwyer HA, Cheer AY, Barakat AI, Rutaganira T. (2002) .Unsteady and three-dimensional simulation of blood flow in the human aortic arch. **J Biomech Eng;124(4):**378—87.

Shipkowitz, T.; Rodgers, V.; Frazin, L. & Chandran, K. (1998). Numerical study on the effect of steady axial flow development in the human aorta on local shear stresses in abdominal aortic branches**. journal of Biomechanics**, Vol. 31, 995-1007.

Shipkowitz, T.; Rodgers, V.; Frazin, L. & Chandran, K. (2000). Numerical study on the effect of secondary flow in the human aorta on local shear stresses in abdominal aortic branches**. journal of Biomechanics**, Vol. 33, 717-728.

Stanworth D R, Johns P. (1977)Ultracentrifugal methods of detecting soluble immune complexes. **Ann Rheum Dis; 36 (suppl)**: 12-16.

Sinha AA, Lopez MT, McDevitt HO. (1990) Autoimmune diseases: the failure of self tolerance. **Science;248**:1380-8.

Steinman, D.; Frayne, R.; Zhang, X.; Rutt, B. & Ethier, C. (1996). MR measurement and numerical simulation of steady flow in an end-to-side anastomosis model. **journal of Biomechanics**, Vol. 29, 537-542.

Strony J, Beaudoin A, Brands D, Adelman B(1993).Analysis of shear stress and hemodynamic factors in a model of coronary artery stenosis and thrombosis. **American Journal of Physiology**. 265 (Heart circulation Physiology 34):H1787-H1796.

Svetla Petkova, Alamgir Hossain, Jamal Naser, and Enzo Palombo(2003). CFD modelling of blood flow in portal vein hypertension with and without thrombosis. Third International Conference on CFD in the Minerals and Process Industries CSIRO, Melbourne, Australia.

T. Hassan, E. V. Timofeev, T. Saito, H. Shimizu, and M. Ezura,(2004) "Computational Replicas: Anatomic Reconstructions of Cerebral Vessels as Volume Numerical Grids at Three-Dimensional Angiography", **AJNR Am J Neuroradiol**, , pp. 1356–1365.

Tang D, Yang C, Kobayahsi S, Ku DN(2004). Effect of a lipid pool on stress/strain distributions in stenotic arteries: 3-D fluid-solid interactions (FSI) models. **Journal of Biomechanical Engineering.** 126:363-370.

Tannehill JC, Anderson DA, Pletcher RH(1997). Computational Fluid Mechanics and Heat Transfer, 2nd edition.

Taylor and Francis, Philadelphia, PA: Anayiotos AS. Fluid dynamics of a compliant bifurcation model**(**1990)**.** Georgia Institute of Technology Thesis**.**

Taylor, C.; Hughes, T. & Zarins, C. (1998a). Finite element modeling of blood flow in arteries. **computer Methods Appl Mech Energy** , Vol. 158, 155-196 .

Taylor, C.; Hughes, T. & Zarins, C. (1998b). Finite element modeling of three-dimensional pulsatile flow in the abdominal aorta: relevance to atherosclerosis. **Annals of Biomedical Engineering**, Vol. 26, 975-987.

Theophilopoulos, A.N., Wilson, C. B. & Dixon, F.J.(1976) The Raji cell radioimmune assay for detecting immune complexes in human sera**. J. cdin. Invest.** 57, 169.

Urs E Nydegger (1998), Immune Complexes. Central Laboratory of Haematology, Inselspital/University Hospital,Berne, Switzerland.

Varghese, S. & Frankel, S. (2003). Numerical Modeling of pulsatile turbulent flow in stenotic vessels**. Journal of biomechanical engineering**, Vol. 125, 445-460.

Valentino Defazio, Raymond C. Christensen, Timothy J. Regan, Lesem J. Baer, Yoshikazu Morita and Harper K. Hellems (1959). Circulatory Changes in Acute Glomerulonephritis. **Circulation**.20:190-200

Vierendeels JA, Riemslagh K, Dick E (2000) Computer simulation of intraventricular flow and pressure gradients during diastole**. J. Bio-mech. Eng., 122**:667–674.

V. Patnaik, G. Kalsey, and R.K. Singla (2001). Bifurcation Of Axillary Artery In Its 3rd Part - A Case Report, **J. Anat. Soc. India**, vol. 50, pp. 166-169.

Winchester R J, Agnello V, Kunkel H G.(1970).Gamma globulin complexes in synovial fluids of patients with rheumatoid arthritis. Partial characterization and relationship to lowered complement levels**. Clin Exp Immunol; 6**: 689-706.

Watanabe H, Hisada T, Sugiura S, Okada J, Fukunari H (2002) Computer simulation of blood flow, left ventricular wall motion and their interrelationship by fluid-structure interaction finite element method. **JSME Int. J. Ser. C – Mech. Syst. Mach. Elem. Manufact. 45(4)**:1003–1012.

Y, Zhang and W. H. Finlay, (2005)" Measurement of the effect of cartilaginous rings on particle deposition in a proximal lung bifurcation model", **Aerosol Sci. Tech**., pp.394-399.

Yoshiyuki Tokuda a, Min-Ho Song a, Yuichi Ueda b, Akihiko Usui b, Toshiaki Akita b, Shigeru Yoneyama c, Shigeru Maruyama d.(2008). Three-dimensional numerical simulation of blood flow in the aortic arch during cardiopulmonary bypass. Effect of increased severity in patient specific stenosis of common carotid artery using CFD—a case study**. European Journal of Cardio-thoracic Surgery**. 33 164—167.

Zvaifler N J.(1974) Rheumatoid synovitis: an extravascular immune complex disease. **Arthritis Rheum; 17**: 297-305.

Appendix

1. Generalized Navier-Stokes Equation.

$$\rho\left(\frac{\partial \mathbf{v}}{\partial t} + \mathbf{v}\cdot\nabla\mathbf{v}\right) = -\nabla p + \nabla\cdot\mathbf{T} + \mathbf{f},$$

v= flow velocity, P = fluid density, P = pressure, T = (deviatoric) stress tensor, **F=** body forces (per unit volume) acting on the fluid, ∇= deloperator.

2. Generalized Euler's Equation.

In differential form, the equations are:

$$\frac{\partial \rho}{\partial t} + \nabla\cdot(\rho\mathbf{u}) = 0$$

$$\frac{\partial \rho\mathbf{u}}{\partial t} + \nabla\cdot(\mathbf{u}\otimes(\rho\mathbf{u})) + \nabla p = \mathbf{0}$$

$$\frac{\partial E}{\partial t} + \nabla\cdot(\mathbf{u}(E+p)) = 0,$$

ρ= is the fluid mass density, ***u***= fluid velocity vector, with components u, v, and w, $E = \rho\, e + \frac{1}{2}\rho\,(u^2 + v^2 + w^2)$ is the total energy per unit volume, with e being the internal energy per unit mass for the fluid, p=pressure, $\otimes$ =Tensor product, $\mathbf{0}$= Zero vector.

3. Generalized Continuity Equation.

$$\frac{\partial \varphi}{\partial t} + \nabla\cdot\mathbf{f} = \sigma$$

∇=divergence, t = time, σ=Generation of q per unit volume per unit time. Terms that generate ($\sigma > 0$) or remove ($\sigma < 0$) q are referred to as a "sources" and "sinks" respectively.

$$\varphi = \frac{\mathrm{d}q}{\mathrm{d}V},$$

q = Scalar variable, V = Volume.

4. System Configurations:
   Microsoft Windows 7, 4 GB RAM, Intel® Core™ 2 DUO Processor T6570 @2.10 GHz 2.10. GHz, 32 BIT Operating System.

5. Exceed 13 x86+x64 Hummingbird package, Fluent 6.2.